Powder Metallurgy Processing of an Al-0.7Mg-0.4Si-(Sn) Alloy

by

Conner Spence

Submitted in partial fulfilment of the requirements
for the degree of Master of Applied Science

at

Dalhousie University
Halifax, Nova Scotia

May 2022

Table of Contents

List of Tables

List of Figures

Abstract

The purpose of this study was to analyze the viability of a powder metallurgy (PM) counterpart to aluminum alloy 6063. 6xxx series (Al-Mg-Si) wrought alloys represent one of the most widely used systems for automotive applications, offering an advantageous balance of thermal conductivity, formability, and strength. The capabilities of 6xxx series alloys is matched by their breadth of variation, with over 45 unique 6xxx alloy chemistries available to meet a vast range of needs. However, in the PM sector there is only one 6xxx series equivalent, PM6061, leading to far more limited viability of the series for aluminum PM manufacturing. To address this shortcoming, research in this project seeks to devise PM systems that are lean in Mg/Si contents so as to invoke maximum thermal conductivity. Four variations of a chemistry comparable to wrought alloy 6063 (Al-0.7Mg-0.5Si) were investigated for this purpose using commercially available powders, with additions of elemental tin powder to aid in the sintering process. The response of these material chemistries to press-and-sinter processing was studied across a range of manufacturing parameters and temper states. Primary analysis first investigated the impact of variations in key PM processing parameters (compaction pressure, sintering temperature, sintering time), and then proceeded to analyzing the sizing response and impact of varied heat treatments, namely the T2 and T8 temper states. Analysis of the resulting product included evaluation of mechanical as well as thermal characteristics, such as microstructural analysis, density measurement, hardness and tensile property measurement, thermal diffusivity testing, thermal expansion testing, and specific heat capacity determination. These analysis steps allowed both for optimal mechanical properties to be identified, as well as for the determination of thermal conductivity of the chemistries across various conditions. The chemistry containing no tin performed poorly throughout all stages of analysis, maintaining a high degree of porosity and presenting the worst mechanical as well as thermal properties across all manufacturing parameters and temper states. Select tin-bearing formulations achieved >99% theoretical density, and peak thermal conductivities that very closely match those of the wrought equivalent.

List of Abbreviations Used

CTE	Coefficient of Thermal Expansion
DSC	Differential Scanning Calorimetry
LFA	Laser Flash Analysis
LPS	Liquid Phase Sintering
OAL	Overall Length
PM	Powder Metallurgy
UTS	Ultimate Tensile Strength
wt.%	Weight Percent

Acknowledgements

I would like to thank Dr. Paul Bishop for the guidance and support provided throughout the completion of this work, as well as the other members of the examining committee Mr. Ian Donaldson and Dr. Graham Gagnon, for their support and insights.

Finally I would like to thank all of my colleagues for all of their assistance and training throughout my time at Dalhousie University. I would like to give special thanks to Mr. Randy Cooke, Dr. Addison Rayner, Mr. Mark MacDonald and Ms. Patricia Scallion for the assistance they have provided across each stage of this process, and their constant willingness to answer questions and provide advice and guidance.

CHAPTER 1 – INTRODUCTION

1.1 Aluminum Powder Metallurgy

1.1.1 Metal Powder Production

In aluminum powder metallurgy (PM), elemental aluminum powder is very frequently used to provide the base aluminum component of the alloy chemistry being utilized. Even in cases where master alloy powders are being used to introduce alloying additions, the bulk will still generally be made up of elemental powders. At both the commercial level and the laboratory level, elemental aluminum powders are typically gas atomized, and specifically air atomized. Inert gas atomized aluminum is also occasionally used, but the increased expense of producing such a powder and preserving the benefits of using an inert gas diminish its frequency of use.

Depending on the desired characteristics, design qualities, and many other factors, atomization systems for aluminum can take a multitude of forms – all effective at producing a powdered aluminum product. Figure 1 identifies the major components of a vertical gas atomization system, and can be considered a reasonable example of a system that would function for the production of aluminum powders [1]. It is worth considering that while this basic layout is applicable, there are a vast range of components used commercially for production of aluminum powders, especially when it comes to nozzles for delivering the melt and gas to their point of interaction [2]. The operation of a system such as the example presented in Figure 1 utilizes a constant flow of pressurized gas to vaporize a stream of molten aluminum, this stream being drawn from a larger chamber of molten aluminum being held at a controlled target temperature. The pressurized gas breaks this stream into small droplets, and these droplets are then allowed to cool as they fall to the collection chamber below. The system utilizes a recirculation system for the gas used, and thus relies on a cyclone separator to remove any extremely fine particles prior to the exhaust gas being reintroduced into the atomization line [1].

1
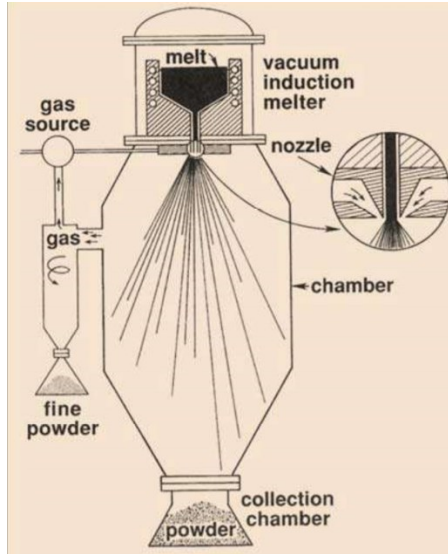
Figure 1: Simplified schematic of a vertical gas atomizer [1]

In gas atomized aluminum, the morphology of the powder particles is heavily dependent on the oxygen partial pressure of the gas being utilized. Here, higher concentrations of oxygen lead to the development of thicker oxide layers on the particles, which impede the formation of spherical morphology before solidification concludes. Thus, as seen in Figure 2 (a), air atomized aluminum powders have an irregular morphology while those that are inert gas atomized present more spherical morphology (Figure 2 (b)) [2]–[4].
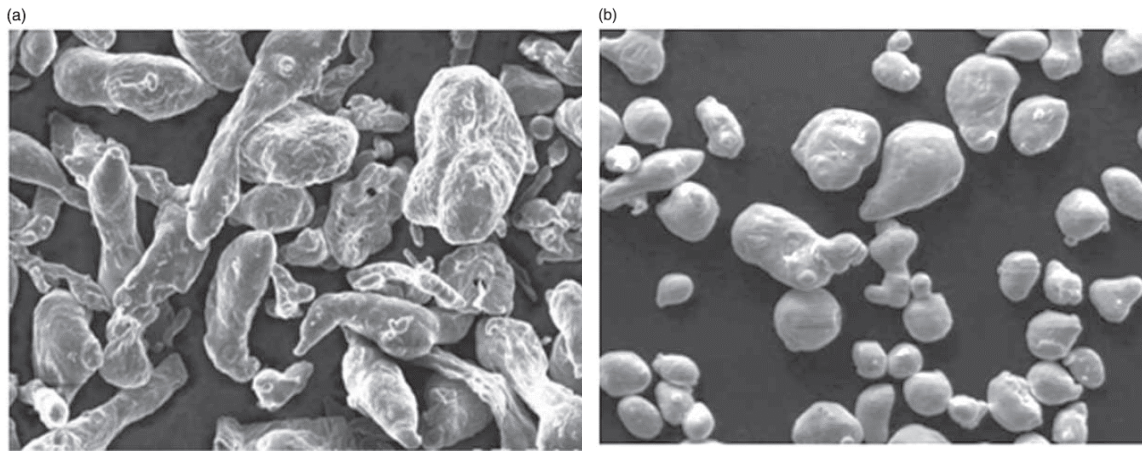
Figure 2: SEM images of typical atomized aluminum powders, a) air atomized, (b) inert gas atomized [4]

In addition to gas atomization, there are a number of other more niche methods that can be used to produce aluminum powder. Alternative methods including centrifugal atomization and melt spinning, along with ultrasonic atomization, can produce specialized particle morphologies but are not known to offer any significant benefit in the press and sinter processing of aluminum. Therefore these methods, while functional, are not used commercially due to the significant increase in powder production costs [2].

When developing an alloy chemistry for aluminum PM – be it an analogue of a pre-existing wrought alloy or a novel alloy system specifically designed for PM efficacy – the inclusion of multiple alloying additions will always be required. There are multiple means of achieving a desired alloy composition, and selection depends on a number of considerations that will be explored at a later point. But regardless of how they will be included, the production of alloying addition powders is consistent for each addition.

Copper is a common alloying element in wrought aluminum alloys and this extends to PM systems just as well. There is a range of production methods for copper powders, all with value. As with most metal powders, gas atomization is a popular means for copper powder production due to the relatively straightforward processing method and high production

rates [5], [6]. Copper powders can also be produced electrolytically, yielding unique dendritic-shaped particles – a morphology entirely unattainable through any other process [7]. Copper is also frequently included in aluminum PM systems in the form of an Al-Cu master alloy, and in these cases the pre-alloyed melt is atomized in a similar fashion to elemental powders [8], [9].

Silicon is another widely utilized aluminum alloying addition both in wrought and PM systems. Unlike metallic alloying additions however, silicon is not a material that is at all conducive to atomization techniques for powder production. Additions of elemental silicon are almost exclusively powders produced through mechanical milling methods, effectively grinding portions of silicon to a particle size acceptable for PM processing [5]–[7]. Another frequently used method for adding silicon to the alloy system is through the use of an Al-Si master alloy powder, which unlike elemental silicon is very conducive to conventional gas atomization techniques [7].

Magnesium is yet another common alloying addition in wrought aluminum alloys, but in aluminum PM it is even more widely utilized due to the significant benefits it offers for the sinterability of aluminum powders, as will be explained in a later section. Magnesium powders can be produced in a range of ways, depending on the needs of the system and process in question. Inert gas atomization is used frequently to produce spherical powder particles [8], [10]. However, magnesium powders may also be produced through mechanical milling, which produces far more irregular angular particles [5], [6], [11], [12]. Examples of these morphologies are shown in Figure 3.
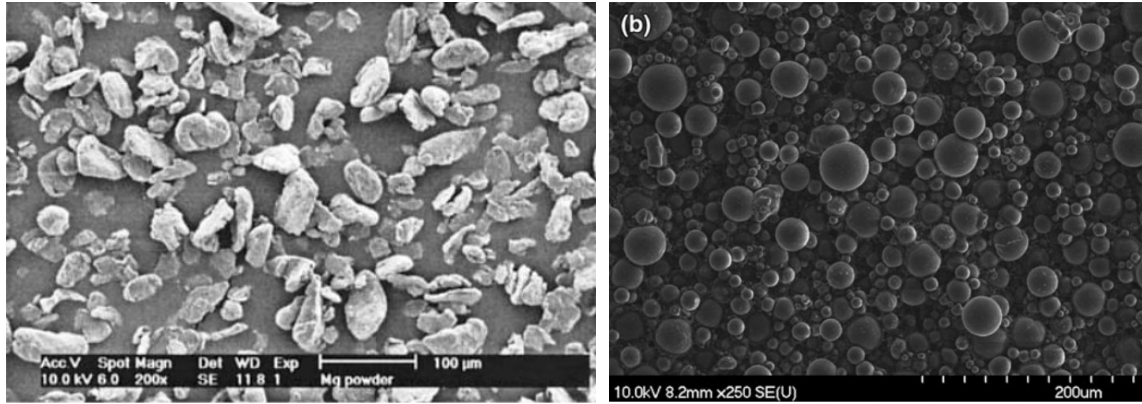
Figure 3: (a) Mechanically milled magnesium powder [12], (b) Inert gas atomized magnesium powder [10]

Tin is a unique alloying addition in that it is common to most aluminum PM systems as it provides unique and valuable benefits for the sinterability. However, it is rarely encountered in wrought alloys. To date, tin has been exclusively utilized as an elemental admixed addition, and is produced via either inert gas atomization [8], [10], or air atomization [5], [11].

1.1.2 Blending & Compaction

At a laboratory scale, blending is often completed with a Turbula® Powder Blender [7]–[11], [13]–[15]. At a commercial scale either diffusion, convection, or shear mixing are generally utilized, where diffusion is a rotating drum, convection is screw mixer, and shear is a blade mixer. Actual blending often takes place in rotating containers that may be of varied shapes, such as cylindrical or double-conical, and which contain baffles, additional spinning blades, and dividers, to assist with intermixing [1], [2].

Segregation of a properly blended powder is a concern regardless of the blending method, and care should be taken to minimize it. While particle size, density, and shape all contribute to segregation, particle size is the primary driving factor – small particles are able to pass through voids between larger particles. Minimizing bulk powder agitation after

blending is complete can assist in alleviating this, as can the inclusion of wetting agents when applicable [1], [2].

The incorporation of a lubricant within aluminum powder blends is required for effective die compaction. Typically, this is an admixed lubricant powder that is added during the blending stage. The nature and quantity of the lubricant used will affect the powder processability, along with the green and sintered properties, and so needs to be considered when preparing a powder blend. The need for admixed lubricants to be burned off prior to actual sintering also presents risks of increased porosity and dimensional change [2], [16].

Once a homogenous, lubricant-laden blend is produced, it is then amenable for the next stage of PM processing – die compaction. Commercially, both mechanical and hydraulic presses are utilized for the powder compaction process. Mechanical presses cannot provide compaction pressures as high as hydraulic press systems, but present the value of significantly higher stroke rates, providing far greater throughput in cases where a lower compaction pressure and time is still capable of producing parts of the desired quality. Hydraulic press systems are capable of much greater compaction pressures, which can allow for longer parts in the pressing direction to be compacted and still achieve the desired density. The lower speed reduces throughput, but also allows a longer time for trapped air within larger parts to escape through the tooling tolerances [2].

1.1.3 Sintering

Aluminum sintering occurs in the presence of a liquid phase for part if not all of the duration of the isothermal hold at peak temperature. This liquid phase can, for appropriate chemistries, facilitate densification both mechanically and via dramatically increased diffusion in comparison to classical solid state sintering. The viability of liquid phase sintering (LPS) is dependent on a number of driving factors; solubilities, wettability and spreading, dihedral angles, and capillary forces. The first consideration when developing an alloy system for LPS is the solubilities at play – both of the base material in the liquid phase material, and of the liquid in the base material. The solubility of the base material in

the liquid is the defining factor in whether this is an effective LPS composition or not, as high solubility and diffusivity are required for the effective diffusion of the base material through the liquid to progress sintering. The solubility of the liquid in the base material is the defining factor in which form of LPS will occur [1], [17].

Wettability is a characteristic that is dependent on the surface energies between the solid, liquid, and gaseous atmosphere. Its principal role is to facilitate spreading of the liquid phase throughout the powder compact. This is important because liquid often forms initially in localized regions of the microstructure, and also because good wettability ensures good contact between the solid and liquid ensuring optimal diffusion opportunity. With a wetting liquid, capillary forces will draw the liquid into the spaces between particles, and this simultaneously exerts a very strong force on the solid particles that may induce particle rearrangement to further densification. The dihedral angle is the angle that occurs at the intersection between a grain boundary and the liquid phase. A low dihedral angle increases the likelihood that the liquid phase will penetrate the grain boundaries within the solid particles themselves, assisting in particle fragmentation and thus densification. Figure 4 provides illustrative examples of good versus bad wetting characteristics of liquid on a solid surface, as well as an illustration of dihedral angle as would be found where two powder particles meet. [1], [17].
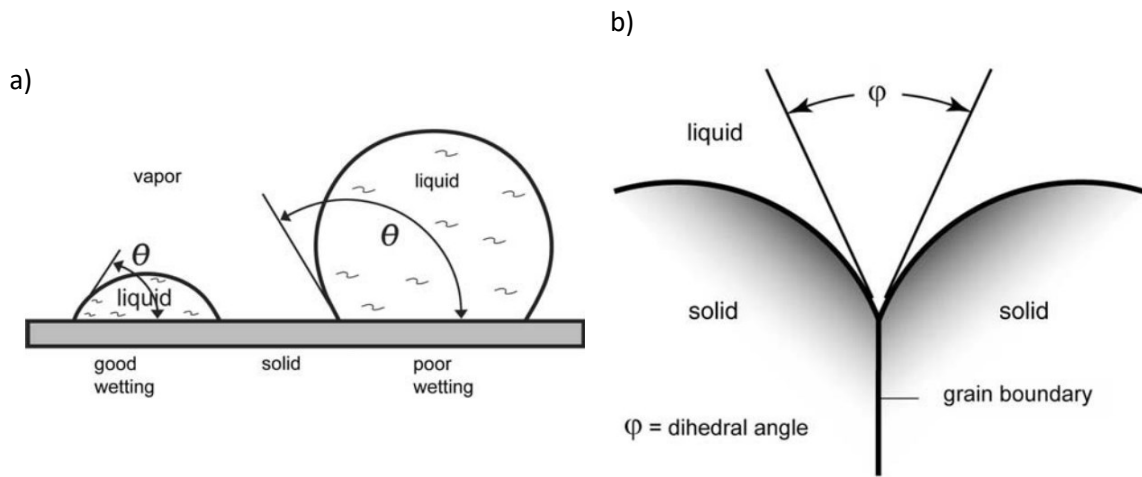
Figure 4: a) Diagram demonstrating good vs. poor wetting characteristics, b) diagram defining a dihedral angle [17]

There are a number of concerns that need to be kept in mind when utilizing LPS. The first is the increased risk of excessive grain growth due to Oswald Ripening, which can potentially degrade the mechanical properties of the finished product even if a high degree of densification is achieved. Additionally, mechanical properties may also be negatively impacted by the formation of brittle phases along grain boundaries as remaining liquid solidifies at the conclusion of sintering. LPS also presents a higher likelihood of prominent distortion due to excessive liquid formation, lack of wettability, solubility imbalances, or slumping [17].

Working windows for specific alloys should provide reasonable boundaries for sintering temperature and time to allow for optimal densification while avoiding excessive grain growth or distortion. Issues of brittle phase formation and inherent limitations in high temperature applications are more difficult to alleviate, and generally require chemistry manipulation. The benefits of further additions or quantity changes need to be balanced with the inevitable change in final properties, but it is often worth the work involved to produce more viable fully sintered parts [17].

There are three main forms of LPS; supersolidus liquid phase sintering, persistent liquid phase sintering, and transient liquid phase sintering. Supersolidus LPS occurs with prealloyed powders, and involves heating the powder to a temperature between the solidus and liquidus temperature of the alloy. Often times these limits need to be determined through the use of Differential Thermal Analysis (DTA) or Differential Scanning Calorimetry (DSC) since phase diagrams for complex chemistries – such as prealloyed analogues of wrought alloys – are rarely available. In this form of LPS, the liquid forms along the grain boundaries of each particle, which then leads to their fragmentation into individual grains, providing greater densification potential [17]. Diffusion of the liquid into the solid base is not a concern in this case, as the base material is partially melting to provide the liquid in the first place. Supersolidus LPS is the predominant mechanism when sintering prealloyed powders [12], [14], [15], [17]–[19], however when there are also alloying additions, for example tin or lead as a sintering aid, the progression is made more complex with the earlier formation of persistent or transient liquid phases before the supersolidus system takes over.

The solubility of the liquid in the base determines whether the liquid phase is transient or persistent. Assuming all other driving factors are met, persistent liquid phase sintering occurs when the liquid phase chemistry has low-to-no solid solubility in the base material at the sintering temperature thereby rendering it as a stable phase. An example can be seen with the Al-Sn system, the phase diagram for which can be found in Figure 5. To be an effective LPS system, the base must still have high solubility in the liquid for effective dissolution of the base in regions of high surface energy and the subsequent re-precipitation.
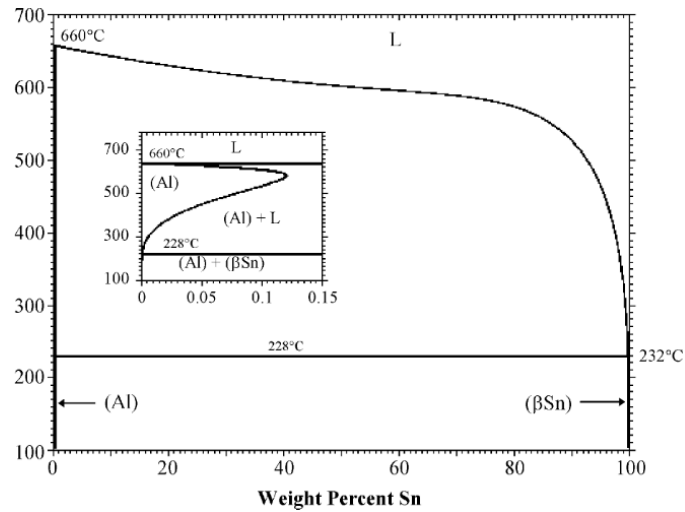
Figure 5: Al-Sn Phase Diagram [20]

In contrast, transient LPS occurs when the liquid phase chemistry has adequate solid solubility in the base as to eventually diffuse into the base material prior to the completion of sintering. I.e., the equilibrium state of the system at the sintering temperature is a solid state system, and the sintering persists long enough for this equilibrium to be reached. An example of such a system can be seen in Figure 6 with the Al-Mg system. Transient liquid phases are generally not ideal for densification, as the lack of persistence often precludes the achievement of peak density.
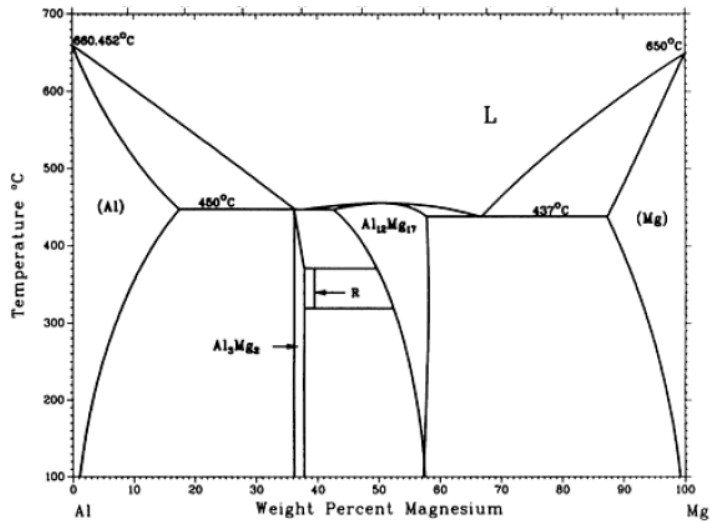
Figure 6: Al-Mg Phase Diagram [20]

The atmosphere within the sintering furnace is a further factor that requires consideration when sintering aluminum. Much of the analysis on this subject focuses on the use of nitrogen, argon, and hydrogen atmospheres as well as blends of those gasses, along with sintering under vacuum. Some have examined the atmospheric effects on the sintering of pure aluminum [21], [22], while others have examined the atmosphere's effect on a relatively wide range of chemistries [13], [19], [23]. The impacts each of these atmospheres have on the sintering of aluminum are generally consistent across alloy chemistries. First and foremost, nitrogen atmospheres impart the greatest sintering response for aluminum [13], [19], [21]–[23]. In addition, hydrogen is extremely detrimental to sinterability [21], [22] while argon [13], [19], [23] and vacuum [13], [19], [21]–[23] sintering invoke a moderate response. Figure 7 illustrates the difference between samples sintered in argon atmosphere vs nitrogen atmosphere, and while the argon sample did sinter, the nitrogen sample was able to achieve much greater densification. Additionally, when using nitrogen as the baseline, nitrogen-hydrogen gas mixes see drastic reductions in sinterability even when hydrogen is present in only very small quantities [21], [22]. Nitrogen-argon mixes also see decreases in sinterability, though argon is not as

11

detrimental and requires greater concentrations before it begins to have a negative impact [21], [22].
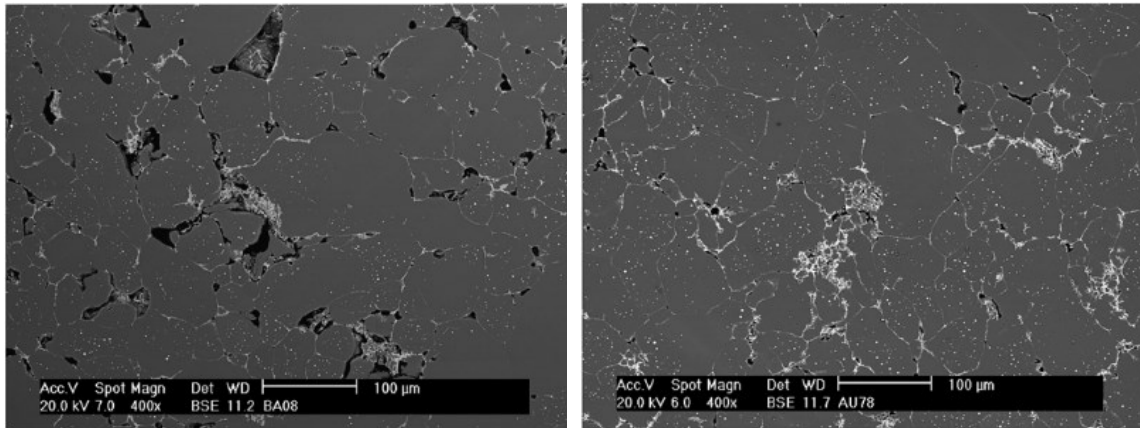
Figure 7: Al-3.8Cu-1Mg-0.7Si-0.1Sn Sintered at 590 °C in a) Argon, b) Nitrogen [13]

Nitrogen is invariably the atmosphere of choice for aluminum sintering, though it is not without potential challenges. Aluminum nitride (AlN) formation may occur when sintering under a nitrogen atmosphere, through nitrogen reacting with aluminum or the aluminum oxide layer [13], [19], [21]–[23]. Internal nitriding may consume nitrogen in pores, and in closed pores this increases ΔP between $P_{furnace}$ and P_{pore}, increasing the sintering stresses on such pores and potentially facilitating shrinkage [13]. Nitridation can also be inhibited through the inclusion of certain alloying additions.

Many of the frequent alloying additions used in aluminum PM are also common additions that have been used in wrought aluminum alloys for very long periods of time. In many cases these additions offer the same mechanical benefits as in the wrought alloy in fully sintered parts, though the nature of sintering and particularly LPS requires additional consideration with regards to what alloying additions can be used, and how they will impact the sintering process. What's more, LPS processing can often utilize new alloying additions that are not frequently used in wrought alloys, due to the vastly different requirements for LPS to be effective.

12

Copper is a widely used alloying addition in wrought aluminum alloys, and its inclusion is the basis of the 2xxx-series of aluminum alloy chemistries. Copper additions in PM applications offer much the same mechanical benefits as wrought alloy systems, when present in fully sintered samples [5], [6], [8]. Magnesium is another addition that is widely used in wrought aluminum alloys, either as the sole primary addition in 5xxx-series alloys or in conjunction with silicon in 6xxx-series alloys. It is similarly widely used in aluminum PM applications, though it's value is actually even greater in terms of PM [11], [13], [23]–[26]. The significant value of magnesium in PM systems in particular is its ability to disrupt the aluminum oxide layer on the surfaces of powder particles. This effect can be optimized with as little as 0.1-1.0wt.% magnesium, and will typically manifest the development of spinel ($MgAl_2O_4$) [11], [13], [23]–[26] thereby disrupting the otherwise continuous shell of Al_2O_3. It can also act to reduce local P_{O2} by acting as a potent oxygen getter [25], [26]. Such phenomena are integral to effective aluminum sintering, as otherwise the oxide greatly inhibits direct metal to metal contact and effective diffusion of aluminum and other alloying additions throughout the system during sintering.

Tin exhibits virtually all features of an ideal LPS system when included with aluminum [5], [13], [18], [23], [24], [27]. It has a melting temperature of 232°C, much lower than aluminum (660°C) and has nearly no solid solubility in aluminum (<0.15%), while aluminum is highly soluble in liquid tin. Additionally, aluminum diffusivity in liquid tin is far greater than in liquid copper. In conjunction with magnesium, tin provides excellent liquid phase sintering support. In Al-Cu systems, tin has a higher diffusivity in Al, allowing it to more quickly bind to vacancies and reduce the rate of copper diffusion – delaying the sometimes transient nature of liquid in such systems [5], [6]. Furthermore, it is also suggested that tin may limit the formation of aluminum nitride during sintering in nitrogen atmospheres [13]. While tin additions do not contribute directly to improvements in mechanical properties, they often serve as an effective sintering aid.

13

1.1.4 Post-Sinter Processing

After sintering is completed, there is almost always some form of post-processing prior to end use deployment. Sizing is a very frequently used finishing operation as it allows for the achievement of tight dimensional tolerances, enhanced surface finish, and frequently, improved density and mechanical properties [9], [28], [29]. Sizing is a cold forming operation that is applied to sintered parts, often immediately after sintering has concluded. The process is typically conducted at room temperature using rigid tooling and press systems comparable to those used during powder compaction [9]. These presses will utilize die sets that correspond very closely to the dimensions of the intended product, though analysis will need to be conducted prior to bulk production to ensure that consistent dimensional changes during sintering can be identified and accounted for when preparing the tooling.

It is generally desirable to complete sizing before post-sinter natural age hardening can take place as this decreases ductility and increases the propensity for component fracture [9], [28], [29]. Distortion and warping, or inconsistent dimensional change between parts, can render sizing impossible [9], [29]. Hence, sizing also requires a high degree of consistency in sintered parts. While post-sinter hardening is inevitable, effort can be made to consider manipulations to the alloy chemistry such that the onset of hardening may be delayed, or that the initial aging does not considerably impact hardness. This is a challenging task, as the powder blend must also maintain the means to produce adequate green strength and sintering response, and thus final properties [9].

In many cases, heat treatment options are considered in conjunction with sizing operations. In these cases the interactions between the two processes, their influence on each other, and the interactions of their results, must be weighed to identify the optimal order of operations as well as the actual parameters to be used. A possible concern for cases when sizing is conducted before heat treatment, is that any microstructural changes caused by the sizing-induced cold work would be largely annihilated, eliminating the mechanical property gains from sizing. In addition to this, the part may suffer from quench-induced distortion with no sizing operation to correct for it [29]. Sizing within treatment stages –

for example after solutionizing and quenching but before any artificial aging – would allow the sizing operation to correct for any quench-induced distortion while the material is still malleable, arriving at what would essentially be a T8 temper [29]. Figure 8 demonstrates a comparison in the sizing response for a PM7075 alloy processed through each of the aforementioned orders of operations. When sizing proceeded solutionization, a much higher pressure was required to achieve appreciable plastic deformation due to the material already being in a naturally aged state. Whereas when sizing immediately followed solutionization, a majority of the preexisting strengthening features have been eliminated which improved formability [29].
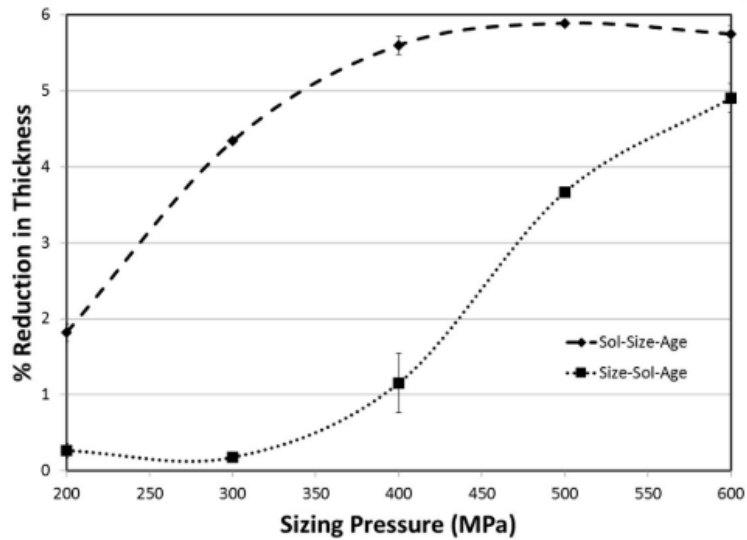
Figure 8: Effect of sizing pressure on percent reduction in thickness of PM7075 aluminum alloy samples for Solutionize-Size-Age (Sol-Size-Age) and Size-solutionize-age (Size-Sol-Age) processing sequences [29]

1.2 6xxx Series Aluminum Alloys

1.2.1 Precipitation Hardening Process

Precipitation hardening is the process of strengthening a material via heat treatment processes that cause a constituent phase to precipitate out of solid solution. Precipitation hardenable alloys, which also can be referred to as "heat treatable" alloys when discussing aluminum, require that the alloy system has a temperature-dependent equilibrium solid solubility gradient. This means that at elevated temperatures the system can be solutionized into a single phase without melting, and with reducing temperature the solid solubility of the precipitate constituents drops to the point that they precipitate out of solution. For example, Figure 9 presents the aluminum rich end of the aluminum copper binary system, a system that provides excellent precipitation hardenability characteristics as described. Figure 10 on the other hand, presenting the aluminum manganese system, is an example of a binary system incapable of producing an appreciable precipitation response.
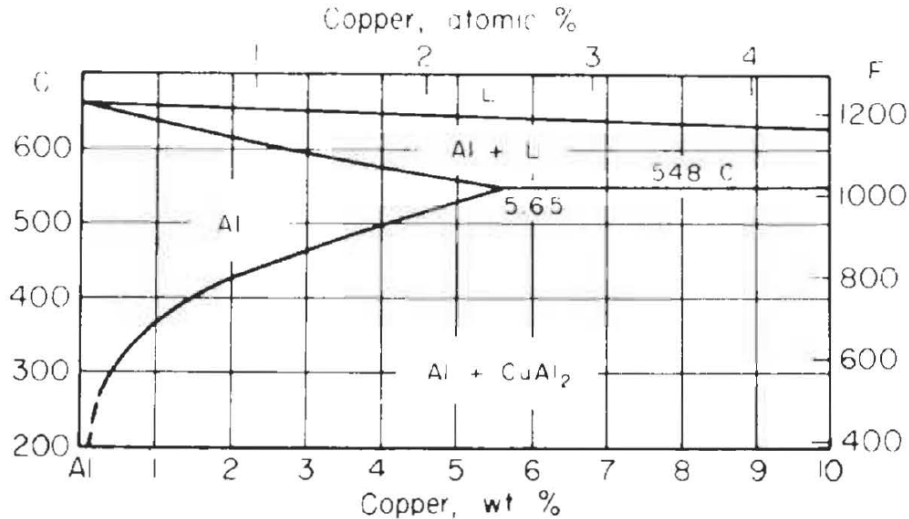
Figure 9: Aluminum-rich end of the Al-Cu phase diagram [30]
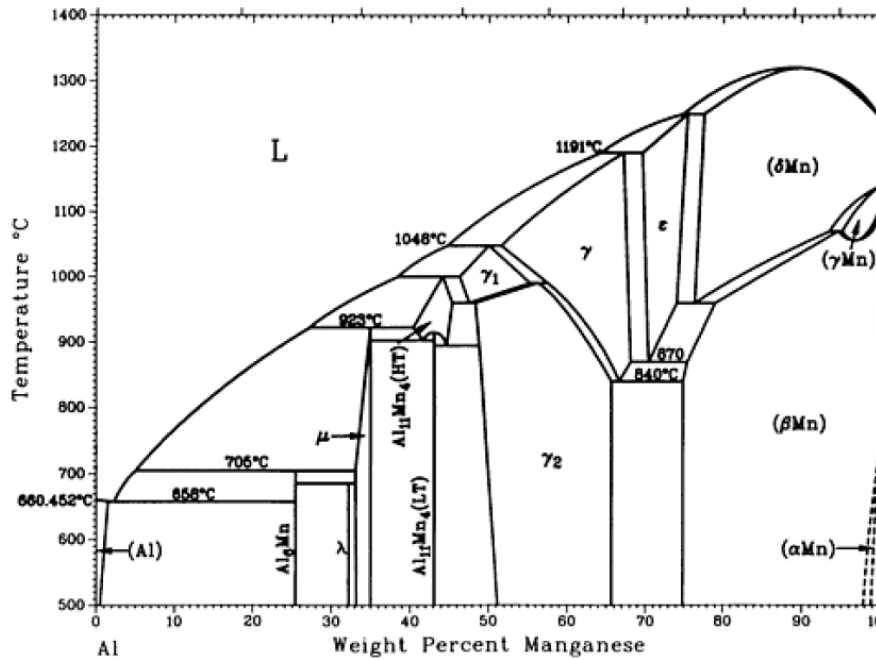
Figure 10: Binary Al-Mn phase diagram [20]

Heat treatment processes for aluminum can follow a multitude of paths, and in fact designations exist for a range of processing paths that do not include heat treatments at all. But in regards to those that do utilize some form of heat treatment, the designations listed in Table 1 describe the treatment process sequence, as well as additional cold working that is also involved in a number of treatment options. The tempering sequence and subsequent designation, as well as the specific temperature, time, and cold work parameters for each stage will vary widely and depend on a range of factors from chemistry to usage case, but the general concepts at play are always the same.

Table 1: List of temper designations [30]

Temper Designation	Description
T1	Cooled from fabrication temperature, naturally aged
T2	Cooled from fabrication temperature, cold worked, naturally aged
T3	Solutionized, cold worked, naturally aged
T4	Solutionized, naturally aged
T5	Cooled from fabrication temperature, artificially aged
T6	Solutionized, artificially aged
T7	Solutionized, stabilized by overaging
T8	Solutionized, cold worked, artificially aged
T9	Solutionized, artificially aged, cold worked
T10	Cooled from fabrication temperature, cold worked, artificially aged

Precipitation hardening occurs in three key steps; Solutionization of the alloy system, quenching to produce a supersaturated solid solution, and then aging to develop precipitates in a prescribed manner to achieve desired properties. Two forms of aging can be utilized - artificial aging and natural aging. Natural aging is the removal of the part from the quench and allowing room temperature precipitate formation over time. Artificial aging instead sees the metal held at an elevated temperature – though still below solutionization temperature – which accelerates the aging process. Control over the aging of a part is often important, and it can be achieved through a variety of methods depending on chemistry and property requirements. Natural aging provides some leeway for mechanical processing of the part in a soft quenched-solutionized state, but also requires much longer periods of time to achieve appropriate strengthening. Artificial aging requires more careful monitoring of time at temperature as overaging can ensue quickly and often leads to a reduction in properties compared to peak. Here, coarsening of precipitate particles will eventually lead to precipitate sizes far larger than is ideal while concurrently reducing the number of precipitates through a process known as Ostwald Ripening. Concerns regarding precipitate size, distribution, and form, will be explored further shortly.

An important consideration when examining the impact that precipitates have on the surrounding bulk matrix, is the type of interface that exists between these features. Categorically, these can be coherent or incoherent interfaces as schematically illustrated in Figure 11. Coherent precipitates have perfect registry with the surrounding lattice, and are "part" of the bulk lattice. In contrast, incoherent precipitates have a distinct boundary between themselves and the bulk crystal lattice [31]. Generally, when a precipitate begins to form it will be coherent. However, lattice strains develop around the precipitate as it grows, since the lattice parameters of it and bulk crystal become increasingly disparate. This strain impedes dislocation motion in the area around these precipitates, contributing to the strengthening of the material even in these early stages [32].

As aging continues and precipitates grow, the coherent precipitate crystal structure changes such that the lattice planes are no longer in perfect registry with those of the bulk metal lattice [33]. Dislocation buildup due to the initial lattice strain also contributes to the formation of a distinct boundary, and the resulting precipitate is a distinctly separate phase. These incoherent particles offer strengthening in multiple ways now that they are distinct from the bulk matrix. Like the coherent counterparts, these particles are also effective at impeding dislocation slip as the particles still produce large matrix distortion in the bulk material. In addition to this however, the particles also provide obstruction due to the fact that dislocations cannot nearly as easily move across the boundary between the bulk and the precipitate due to the discrete change in lattice structure. This strengthening is known as the Orowan hardening mechanism, whereby these dislocations must bend around the particles rather than pass through them [33].
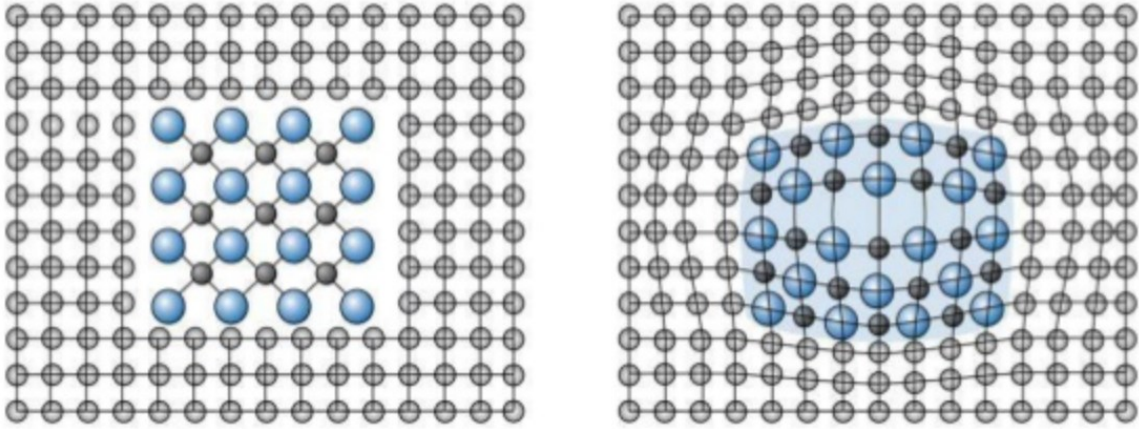
Figure 11: Schematic Diagram of coherent vs. incoherent precipitates [32]

The peak strengthening derived from precipitates generally occurs immediately after the transition from coherent to incoherent precipitate, where the new improvements of the incoherent precipitates can be experienced while still maintaining many very small precipitates dispersed throughout the bulk material. Precipitates throughout the bulk are at no point all the same size, and particle growth does not occur at the same rate at all points. Further aging beyond the point of incoherent boundary formation will lead to coarsening of some particles at the expense of others, leading to an overall reduction in strengthening benefit. This coarsening effect is detrimental because Orowan hardening is most effective with closely spaced particles. With fewer larger precipitates, larger gaps between them exist than with many smaller particles, thus opening up larger regions of the bulk lattice for free dislocation movement [33].

It is impossible to avoid this coarsening effect with continued aging because precipitate formation at different regions within the bulk lattice will always progress at different rates. Most notably, precipitates that initially form at high energy lattice sites such as grain boundaries are more thermodynamically stable than smaller precipitates that form at the interior of the grain. Not only is precipitate nucleation easier in these high energy regions – thus seeing greater precipitate density even at the onset of aging – but their stability and easier growth will lead to the dissolution of nearby smaller particles, the material of which

will diffuse through the lattice and reprecipitate on these larger particles leading to even more coarsening. Figure 12 is a micrograph demonstrating an overaged Al-4%Cu alloy sample. Here, precipitate formation can be seen very clearly at both the grain boundaries, as well as within the bulk of the grains themselves. The micrograph illustrates very well the preferential formation of precipitates in high energy regions like grain boundaries, as these precipitates have demonstrated dramatically greater growth than the precipitates constrained within the bulk.
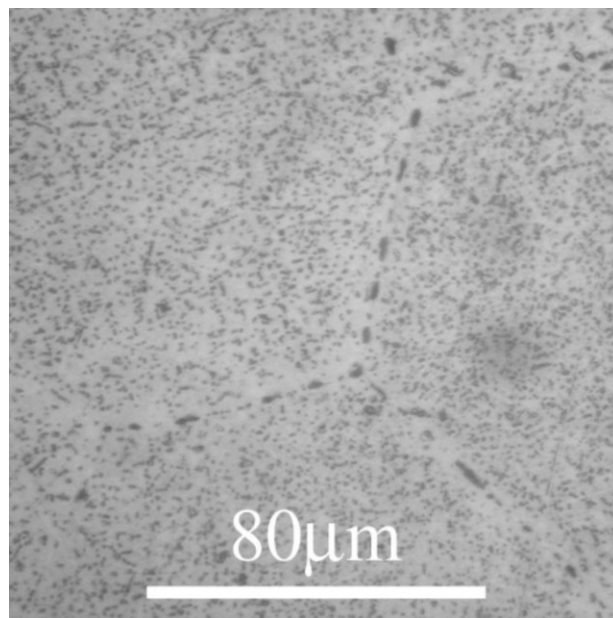
Figure 12: Overaged Al-4%Cu sample - Micrograph demonstrating precipitate formation on grain boundaries and within grains [31]

Regions near grain boundaries are frequently found to have much smaller quantities of precipitates to the point that they can be devoid of precipitates entirely – and these regions are known as precipitate free zones (PFZs). PFZs generally occur for two reasons. First is the fact that precipitates often nucleate on vacancies, and grain boundaries are vacancy sinks. This leads to the regions around grain boundaries being disproportionately vacancy free, which impedes the nucleation of precipitates in the first place. In addition to this, as

mentioned earlier grain boundaries themselves provide high energy lattice sites for precipitate nucleation and easier growth, leading to accelerated coarsening and consumption of nearby solute from the adjacent matrix. The region around the grain boundaries thus does not contain enough solute to invoke precipitate formation [34]. PFZ development can be remedied to a degree in certain cases, but it is not a straightforward process. In the case of vacancy depletion, heat treatment at lower temperatures can facilitate nucleation. The cost of this, however, is significantly reduced precipitation rate requiring unrealistically long treatment times. A two stage heat treatment can partially remedy this new problem by initiating nucleation at lower temperatures before increasing the temperature to grow precipitates, but this still requires a degree of growth at the lower temperature or else the sub-critical sized particles will simply redissolve and deposit on other larger particles. In some chemistries it is also potentially viable to add trace amounts of other alloying additions that may impede vacancy mobility, thus ensuring nucleation and precipitate growth can occur [34].

1.2.2 Aluminum-Magnesium-Silicon System

The precipitation hardening that forms the backbone of strengthening in 6xxx series aluminum is carried out using the same solutionize – quench – age steps discussed above, and is subject to the same limitations, beneficial factors, and considerations explored. For most 6xxx series alloys, the magnesium and silicon content usually resides around 0.6-1.2% and 0.4-1.3%, respectively. More specifically, the ratio of magnesium and silicon frequently lies around the stoichiometric requirements for the formation of magnesium silicide, Mg_2Si. Mg_2Si is the compound that defines the precipitation hardenability of this series of alloys and so ensuring a balance of the two constituents is important to ensure the most effective precipitation can take place. That being said, excess of silicon in particular beyond the stoichiometric requirement form Mg_2Si formation is frequently utilized, and the impacts of this excess is discussed in the following section.

Figure 13 presents a vertical binary section of the aluminum-magnesium-silicon ternary system at the stoichiometric Mg_2Si composition. As Mg_2Si is the strengthening precipitate

in this system, this pseudo-binary phase diagram can be used to identify appropriate chemistries and temperatures for precipitation strengthening treatments.
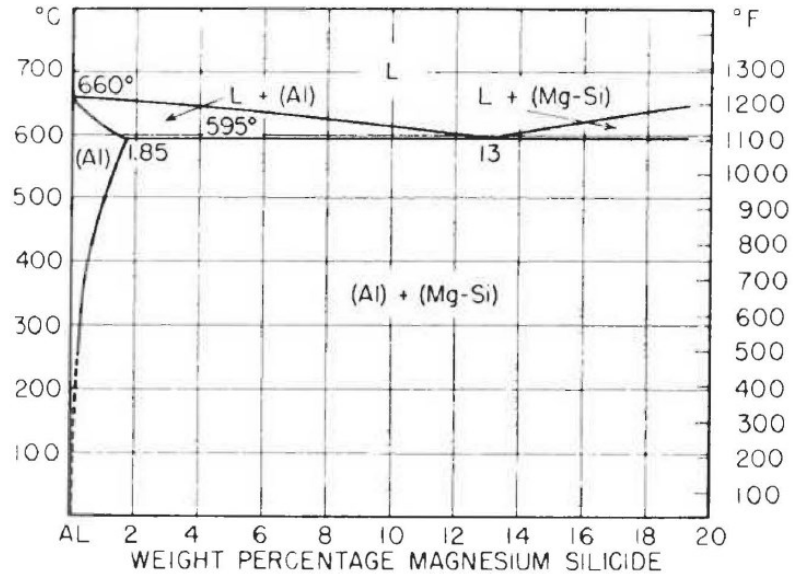
Figure 13: Binary section, aluminum - magnesium silicide (Mg_2Si) phase diagram [30]

While there is still some degree of debate on the fine details of the precipitation sequence in the Al-Mg-Si system, a general outlining description can be stated with more confidence – at least for the pseudo-binary Al-(Mg_2Si) section. Initiating from a supersaturated solid solution, the first stage of precipitation is the discrete clustering of silicon atoms and magnesium atoms. These clusters then lead to the formation of spherical coherent Guinier–Preston zones (GP-zones), that then begin to elongate along the cube matrix direction to produce a needle-like shape. The GP-zones are relatively stable, though with continued aging the GP zones will grow to form coherent β'' precipitates that maintain the needle like shape, and then progressing further form incoherent, rod-shaped β' precipitates – still on a very nanometric scale. The final variant (β phase) is the equilibrium phase that takes the form of incoherent square platelets within the aluminum matrix [4], [35]–[38]. Figure 14 presents a series of TEM micrographs that display the progression of precipitate

23

formation as aging time increases (and in the case of (f), with increasing temperature). Figure 15 presents coarsened β' precipitates that maintain the rod-like shape along the lattice planes. There is observable evidence of precipitates along all three cubic planes, and the lack of square plate precipitates in the plane of viewing suggests that there has not yet been any equilibrium β phase formation yet in this region.
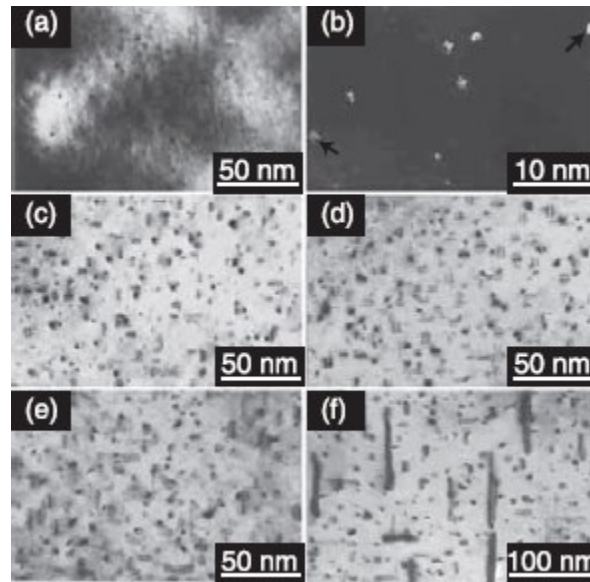
Figure 14: TEM micrographs of 6061 alloy, precipitate dispersion at different stages of artificial aging. (a),(b): 10 minutes at 175°C, (c) 30 minutes at 175°C, (d) 4 hours at 175°C, (e) 72 hours at 175°C, (f) 20 hours at 200°C [4]
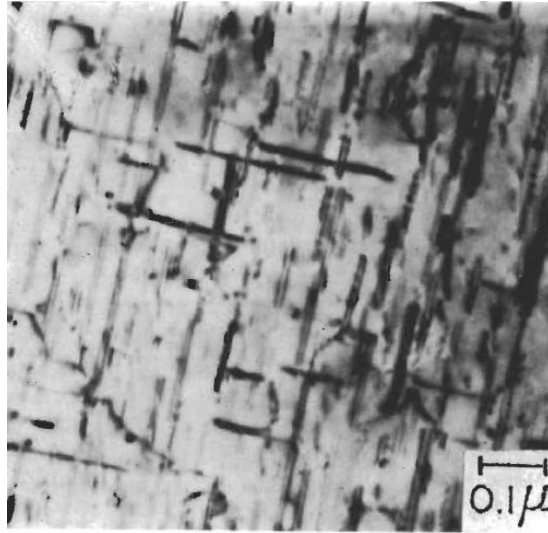
Figure 15: Al-1.3% Mg₂Si aged 24 hours at 160C, reheated for 15 minutes at 275C, presenting coarsened β' precipitates [30]

For the purposes of age hardening, when aging from a perfectly solutionized state the aging process virtually always concludes with the metastable β' phase, as this phase offers the greatest benefits for strengthening. It should be noted that processing techniques that involve high temperatures but not immediate quench after processing, such as a conventional PM sintering cycle, there is inevitably going to be uncontrolled precipitation during cooling that could result in coarsened precipitate particles. This fact must always be taken into consideration when working with such alloys, and emphasizes the importance of the solutionization stage for proper controlled precipitation.

1.2.3 Chemistry Variance: Excesses of Mg or Si, and Other Metal Additions

Variance in chemistry frequently has direct and observable impacts on the properties of an alloy, and 6xxx-series aluminum systems are no exception. Mg_2Si precipitates are the driving means of strengthening in 6xxx-series systems, and the impacts of changing the magnesium and silicon concentrations while maintaining the stoichiometric ratio between the two has been discussed previously. But it is not necessary to maintain that exact

stoichiometric ratio to produce working alloys, and many do include magnesium or more frequently silicon in excess of what is stoichiometrically required. Excess magnesium does not result in any appreciable increase in properties, nor significantly impact the precipitation response [39]. However, silicon has been found to provide a range of changes to both the precipitation response and strengthening effects.

One way of sub-defining 6xxx-series alloys is based on the Mg-Si ratio. A 'balanced alloy' has a ratio of 1.73:1 by weight, which corresponds to the atomic 2:1 ratio of Mg_2Si. Alternatively, a system can be referred to as an 'excess Si alloy', which are systems that have a ratio <1.73 [4]. In terms of the works explored here, the 6xxx-series excess Si alloys are either commercial alloys that have excess Si or modified commercial systems. In both cases the silicon content is in the same relative magnitude as the quantities used to define the 6xxx-series system in the first place, ranging from 0.4% to 1.5% by weight [35], [39]–[42].

Excess silicon does not have a discernable impact on the actual precipitation sequence in Al-Mg-Si systems, so far as to change the order in which precursory precipitates form. It does however impact formation rate and density of precipitates, potentially quite significantly. It has been reported that alloys containing excess Si exhibit a faster age hardening response such that the time to initiate hardening is reduced [40], [41]. It is suggested that this is due to the fact that the chemical composition of atom clustering and the GP zones at the earlier stages of precipitation align with the given chemistry, leading to an increasing density of GP zones as the number of silicon atoms available in the Mg-Si atom clusters increases [41]. This then leads to enhanced precipitation of fine, uniformly distributed β'' particles, enhancing the strengthening effect. This also leads to a reduction in peak strength stability when it comes to the potential for over-aging, which then requires slightly more care in attaining peak strengthening [40]. This lack of stability can be pointed at least in part to the fact that at much lower Mg-Si ratios, it has been found that the precipitation of free silicon also occurs during the precipitation process. This silicon precipitation is observed later in the aging process and is attributed at least in part to partial

dissolution of β'' particles, which suppresses the precipitation of equilibrium Mg_2Si [35], [40].

This potential for accelerated onset of aging can be beneficial in some applications, but does present challenges when it comes to forming or sizing of parts that are still at elevated temperatures when fresh from manufacture, such as PM sintered parts. In cases where this is not a primary concern, the combined potential of accelerated aging and greater number of fine precipitates, if preserved, offers excellent benefits to strengthening.

While magnesium and silicon are always the primary additions in 6xxx-series alloys, it is also common to see further minor alloying additions being made that offer a range of beneficial properties. These benefits sometimes need to be balanced with downsides to their inclusion, but these are regularly dealt with considerations. One of the more common minor additions is copper. As a most basic outline, copper provides enhanced strengthening in these alloy systems, but at a cost of potential reduction in corrosion resistance with increasing concentrations (generally >0.5%) [30]. Copper is an important minor alloying addition because it has a direct impact on the Mg_2Si precipitation sequence, and also spurs the development of alternative precipitates in conjunction to the primary Mg_2Si. First, it has been observed that in chemistries with relatively high copper content, copper atoms were found to manifest a more complicated precipitation sequence, and also the development of a number of additional equilibrium precipitate phases in addition to the β phase. These include θ-phase (Al_2Cu) – which forms the basis of precipitation hardening in 2xxx-series Al-Cu aluminum alloys – and S-phase (Al_2CuMg), which is also a major precipitate in 2xxx-series alloys that also contain magnesium [4], [43]–[45]. A quaternary precipitate phase known as the Q phase, and a precursory metastable Q' phase, can also form. There are various reported stoichiometries for this compound, one of which is $Al_5Cu_2Mg_8Si_6$ [4], [43].

Other minor additions in these alloy systems are chromium and manganese. These additions offer a capacity for increased strengthening along with increased grain size control [30], [46]. This is quite valuable for age hardenable alloy systems where coarsening of grains remains a factor even when precipitate properties may be taking center stage.

1.2.4 Current Wrought and PM utilization of 6xxx Alloys

The 6xxx-series of aluminum alloys contains a wide variety of chemistries, with alloys containing many different combinations of the aforementioned additions alongside the magnesium and silicon that define them. The range of alloys with only magnesium and silicon still includes significant diversity however. One fairly lean example is Al6063, with a typical composition of Al0.7Mg0.4Si. Al6063 is extremely widely used in extrusion applications, in the manufacture of pipes, railings, furniture, and flooring components. Al6063 is also a popular in applications requiring high thermal conductivity, for which depending on the temper it possesses thermal conductivities ranging from 193-218 W/m·K [47]. A fairly common modified version is Al6463, in which the differing factor is the ensuring that iron content stays as low as possible, and must remain below 0.15%. This limitation provides benefits to finishing as well as improves the brightness of the aluminum after anodizing, and so can be found in parts where aesthetics are important alongside the other properties of Al6063 [1]. Another lean example is Al6005, with a typical composition of Al0.8Si0.5Mg, also often used in extruded part applications where greater strength is required, though this does come with a sacrifice in extrudability. Depending on temper, Al6005 can provide yield strengths ranging from 103 to 241 MPa, while Al6063 ranges in yield strength from only 48 to 214 MPa [47].

Many commonly used 6xxx alloys include more than just magnesium and silicon. Al6061, with a typical composition of Al1.0Mg0.6Si0.3Cu0.2Cr is one of the most widely used aluminum alloys in the world. This alloy sees use in a substantial range of structural applications, from vehicle and boat bodies, railroad cars, pipelines, and many others where weldability and strength are required. Depending on temper, Al6061 has yield strengths ranging from 145 to 276 MPa, but this does come at the expense of extrudability. While extrusion of Al6061 is possible and done commercially, it is more commonly forged and manufactured in the form of sheet and plate, rather than more complicated extruded structures. Al6061 is also not ideal for thermal conduction applications with a peak thermal conductivity of only 180 W/m·K – though this can only be achieved with an O temper

which entirely negates any conventional strength benefits 6061 carries. In temper states that allow Al6061 to achieve it's strength, thermal conductivity is in the range of 154 to 167 W/m·K [47]. While many 6xxx alloys are magnesium weighted, there are many that have a surplus of silicon as well. Two such examples are Al6010 and Al6070, with compositions of 0.8Mg1.0Si0.5Mn0.35Cu and 0.8Mg1.4Si0.7Mn0.3Cu. Al6010 is typically used in automobile body sheet, with a yield strength typically around 172 MPa and decent formability. Al6070 on the other hand benefits even more from it's elevated silicon content which provides even greater strength, with yield strengths ranging from 172 to 352 MPa. This strength makes it a popular choice for heavy structural applications, pipelines, and automotive structural components. The thermal conductivity of these alloys suffer from these further additions however, just as with Al6061. If the benefits of these alloys and their additions -their mechanical strength- are to be seen, thermal conductivity suffers, and neither can a conductivity greater than 176 W/m·K [47].

1.3 Thermal Properties of Metals

1.3.1 Heat Capacity and DSC

Heat capacity (C), or thermal capacity, is a physical property of matter defined as the amount of heat to be supplied to a given mass of a material to produce a unit change in its temperature. As a direct continuation of this, specific heat capacity (typically c_p) is the extrinsic form of heat capacity and is defined as the heat capacity divided by the mass of a given sample [48].

$$C = \lim_{\Delta T \to 0} \frac{\Delta Q}{\Delta T} \tag{1}$$

$$c_p = \frac{C}{m} = \frac{1}{m} \cdot \frac{\Delta Q}{\Delta T} \tag{2}$$

$$Q = cm\Delta T \tag{3}$$

29

The equations presented here illustrate these relationships. Equation (1) describes the relationship between heat energy (ΔQ) and sample temperature (ΔT) for the determination of heat capacity (C). Equation (2) then incorporates mass (m) for the determination of specific heat capacity (c_p). Equation (3) is relevant in cases where specific heat capacity is already known, and is most frequently used to calculate the quantity of heat energy entering or leaving a system through measurement of temperature change, while knowing specimen mass.

In the above, specific heat capacity is denoted as "c_p", however this denotation is not always accurate. In reality, the definition and subsequent denotation for specific heat capacity is dependent on the nature of the thermodynamic process involved, such that "specific heat capacity" can have varied meaning. Under isobaric conditions, such that pressure remains constant over testing time, heat energy supplied to the system contributes both to the work done as well as the internal energy of the material. In this situation specific heat capacity is denoted c_p. Under isochoric conditions the constant parameter is volume, thus no work is being done by the energy being added and this supplied heat is only changing the internal energy. Under this condition, specific heat capacity is instead denoted as c_v. Conceptually there is also the idea of an isothermal environment, but in this case where temperature does not change an infinite amount of energy would be required to increase the temperature of the system and thus is not applicable to discussion of heat capacity. That being said, this concept of "infinite" heat capacities does present itself in the situation of phase transition, as the heat is utilized changing the material state rather than raising the temperature [48].

Specific heat capacity of a substance often varies, sometimes substantially, depending on conditions of temperature and pressure. It is also of course impacted by material expansion during heating and a substance's freedom, or lack thereof, to do so. Specific heats of gasses can be measured under isochoric conditions fairly easily, but it is generally challenging and expensive to do so for liquids and solids. Because of this, measured values for materials

in these states are typically generated under a constant pressure environment, leading to c_p virtually always being the heat capacity used.

Also of relevance is consideration of what is actually going on at the atomic level. Heat capacity is a measure of how the material stores energy input as it is being heated, and the ranging capability of different materials to do so directly reflects in their heat capacities. For example, if the molecules in a material may only vibrate, as in a non-metallic crystal structure, then c_p is low, but if they can also rotate and translate within the bulk structure then the c_p would be comparatively higher. Vibrational energy is what is measured as temperature and as such, systems more limited to atomic/molecular vibration over rotational and translational movement present a greater temperature increase when a given amount of energy is added – a lower heat capacity [49].

Differential Scanning Calorimetry (DSC) is a potent thermo-analytical technique, where the difference in heat flow (power) to a sample and a reference is monitored against time or temperature while the temperature of the sample is programmed to follow a given track. These tracks include heating within a wide range of heating rates, isothermal holding, and cooling steps with frequently smaller ranges [49], [50]. Additionally, DSC analysis is carried out in a specified atmosphere, in line with whatever may be deemed necessary for the given application at hand. The differential signal measurement and the dynamic mode of operation are the two most important characteristic features of this process.

Overall performance of DSC, specifically for c_p measurement, requires careful consideration of a range of variables that can be impacted by characteristics of the sample, the system, other apparatus used during testing such as crucibles, and operator actions. All of these considerations can impact the final result and the reproducibility of test; thus, consistency is of utmost importance [51]. A major factor of note, and often a direct focus of DSC analysis, is that when a sample undergoes a physical transformation such as a phase transition, more or less heat will need to flow to it than the reference to maintain both at the same temperature. Whether more or less heat must flow to the sample depends on whether the process that is occurring is endothermic or exothermic in nature. This effect makes DSC extremely effective at identifying phase transitions in materials, the

temperatures at which they occur, the rate of transformation, and the change in thermal properties these new phases may have.

Determination of heat capacity via DSC is based on a number of factors. The process and standards are outlined in ASTM E1269-11 [52]. First, it is required that the heat energy input – specifically the difference between the reference and the given sample – is measured constantly over time to achieve a desired rate of temperature change. Then by extension the changes in the energy required to increase the temperature of a sample can be easily identified. The second consideration for heat capacity measurement, is that it must be determined by comparing a sample to that of a known standard as heat capacity of a material cannot be measured directly.

Due to this requirement, the measuring of heat capacity for a given sample requires a series of tests for accurate determination. The first test establishes the baseline, an indicator for the 'zero-point' for heat capacity at a given temperature. This test identifies the heat capacity of the sample holder or crucible, so that it can be corrected for. Then, a standard sample with a known c_p versus temperature is tested under the same conditions the unknown sample is to be tested under. Typically, synthetic sapphire is used for this purpose as required by the ASTM standard. The third and final test is the sample itself. The following equation (4) can then be used to determine the sample c_p:

$$C_{p\,(s)} = c_{p(st)} \frac{D_s W_{st}}{D_{st} W_s} \tag{4}$$

Where,

$C_{p(st)}$ is the known specific heat capacity of the sapphire standard,

D_s is the vertical displacement between the specimen holder and the specimen DSC thermal curves at a given temperature,

D_{st} is the vertical displacement between the specimen holder and the sapphire DSC thermal curves at a given temperature,

W_s is the mass of the sample,

32

W_{st} is the mass of the standard

Figure 16 presents a schematic of the three test results and indicates D_s and D_{st} as described above for the purpose of c_p calculation. It is highly important to note that this equation only applies when the same crucible has been used for all three tests. Calorimetric sensitivity relating to variance in crucible mass can be accounted for but it requires a more complicated calculation, and avoiding this requirement is preferred [52].
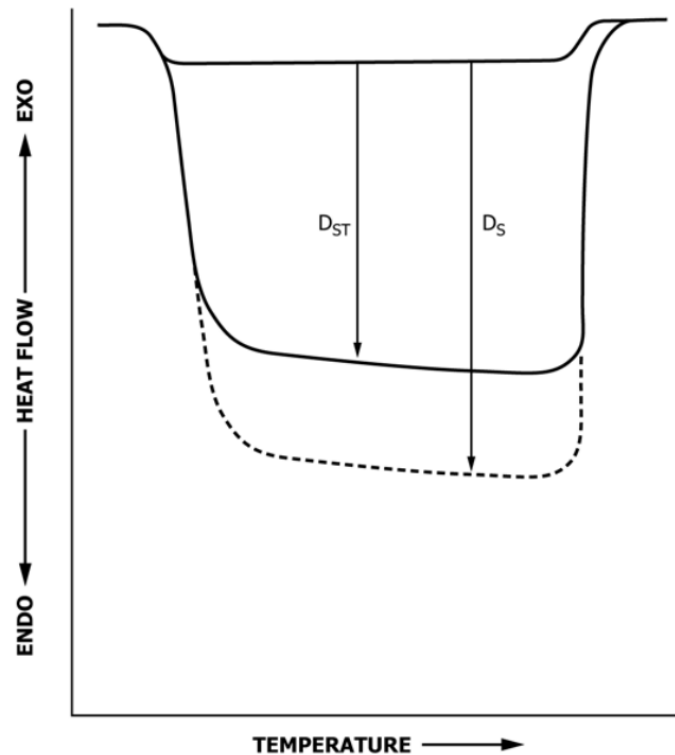
Figure 16: Specific heat capacity thermal curves of empty crucible baseline, standard sapphire, and unknown specimen [52]

1.3.2 Thermal Conductivity, Thermal Diffusivity, and Common Measurement Methods

Thermal conduction is the transfer of internal energy via microscopic collisions between particles and movement of electrons within a body. Thus, the thermal conductivity of a

material is a measure of its ability to conduct this energy [53]. Figure 17 presents a demonstrative schematic to illustrate thermal conduction, and the following is the defining equation (5) for thermal conductivity:

$$q = -k\nabla T \tag{5}$$

Where,

k is the thermal conductivity,

q is the heat flux,

∇T is the given temperature gradient,
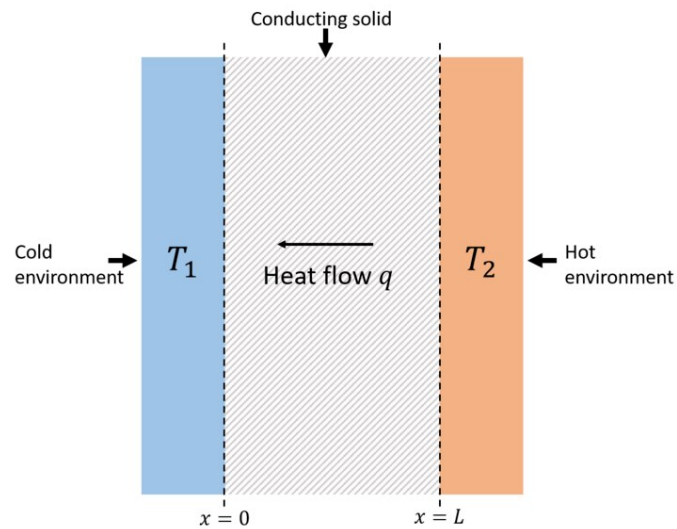
Figure 17: Demonstrative schematic to illustrate thermal conduction [54]

The thermal conductivity of a material is difficult to predict from first-principles, as the mechanisms of thermal conduction from the atomic level on up varies among different materials and material states. There are a wide range of influencing factors that each have their own unique influence depending on the material and surrounding environment. The first such factor is the materials temperature. Temperature impacts the conductivity of

metals and non-metals differently, but in regards to the most relevant in this case, metals, heat conduction is primarily achieved through the movement of free electrons. In accordance with the Wiedemann-Franz law, the thermal conductivity of a material is roughly proportional to the product of absolute temperature and current electrical conductivity [55]. In pure metals, thermal conductivity is relatively constant as a function of temperature. However, in alloyed systems thermal conductivity increases with temperature, often in a directly proportional manner [55].

Another important factor is the occurrence of phase transitions over a prescribed temperature range. These can have dramatic impacts on thermal conductivity, the significance being touched on in the context of heat capacity already. This applies to both physical and allotropic transitions, though physical transitions frequently present more dramatic shifts [53]. Material anisotropy can also impact thermal properties. If a material presents anisotropic qualities, thermal conductivity can vary depending on the axial direction of the crystals. Common scenarios wherein this is observed include metals that have undergone extreme levels of cold forming, or are processed as laminated structures [53]. Magnetic fields can influence the thermal conductivity of a material in some cases as well. A thermal-Hall effect, analogous to the Hall effect, describes the formation of a thermal gradient rather than an electric field when a magnetic field is applied [53]. Occurrence of this in conductors can take the form of the Righi-Leduc effect, for which the application of the magnetic field perpendicular to a thermal gradient produces a new thermal gradient in the direction perpendicular to both the magnetic field and original gradient [56]. Additionally, there also exists the Maggi-Righi-Leduc effect, describing a phenomenon of changing thermal conductivity in the presence of a magnetic field [56].

A final influencing factor on thermal conductivity is the presence of gas pockets within an otherwise well conducting solid material. These features can have deleterious effects on thermal conductivity by obstructing what would otherwise be good heat conduction pathways. This is of course directly relevant and important for consideration when examining the thermal properties of PM materials, illustrating the importance of reducing porosity not just for mechanical gain, but for the benefit of thermal properties as well.

Combining the thermal properties discussed thus far, a third derivative property termed thermal diffusivity can be defined. Thermal Diffusivity is defined as the ratio of the thermal conductivity and the heat storage capability of a material [57]. That is, generally thermal diffusivity is defined not as an independent property but rather a relation between the thermal conductivity of a material and the volumetric heat capacity of a material – which is density times specific heat capacity.

$$\alpha = \frac{k}{\rho c_p} \tag{6}$$

The above equation (6) describes this relation, where,

α is the thermal diffusivity of a material,

k is the thermal conductivity,

c_p is the specific heat capacity,

ρ is the density

Thermal Diffusivity describes the rate of temperature spread through a material, but is not necessarily indicative of how fast the given material can dissipate heat energy. Instead, it provides insight into the "competition" between the conduction and storing of thermal energy, and is related to the speed to reach thermal equilibrium under variable conditions [57].

Techniques for measuring thermal conductivity can generally be broken down into two categories; steady-state and transient. Steady state methods record measurements when the material being testing reaches an equilibrium thermal state; that being the condition attained when the entirety of the sample has a constant temperature that is not changing with time. These systems often prove to be mathematically simpler in use and provide more accurate results than transient systems, but a major disadvantage is that it generally takes a long time to reach the required thermal equilibrium. Transient, or non-steady-state techniques record measurements during the heating process. These methods determine thermal conductivity and related properties through transient sensors, and thus

36

measurements can be made relatively quickly – which is an immense advantage over steady state methodologies. These methods are capable of directly determining thermal diffusivity, and while generally less accurate, the rate of testing advantage is significant enough that the development and use of these systems is very widespread [58].

Figure 18 illustrates four common measurement techniques with each plotted to indicate what ranges in thermal conductivity and temperature they can be utilized for. One concept is a steady state process known as the guarded hot plate, schematically illustrated in Figure 19. This system is the most effective and commonly used apparatus for determining the thermal conductivity of thermally insulating materials. The system relies on a steady temperature difference across a known specimen thickness, and the primary goal is to control the heat flow through the material. A user defined temperature difference is established between the hot and cold plates, and this difference is maintained while a temperature gradient develops within the specimen. This system does, like other steady-state systems, suffer from the fact that it is very slow to achieve an equilibrium state. Once steady-state equilibrium is reached, the power rate input in the hot plate is measured, and it is assumed that the power is entirely transferred across the sample due to the guarded nature of the surrounding hot plates. With this equilibrium state, the thermal conductivity can be calculated from the input values [58].
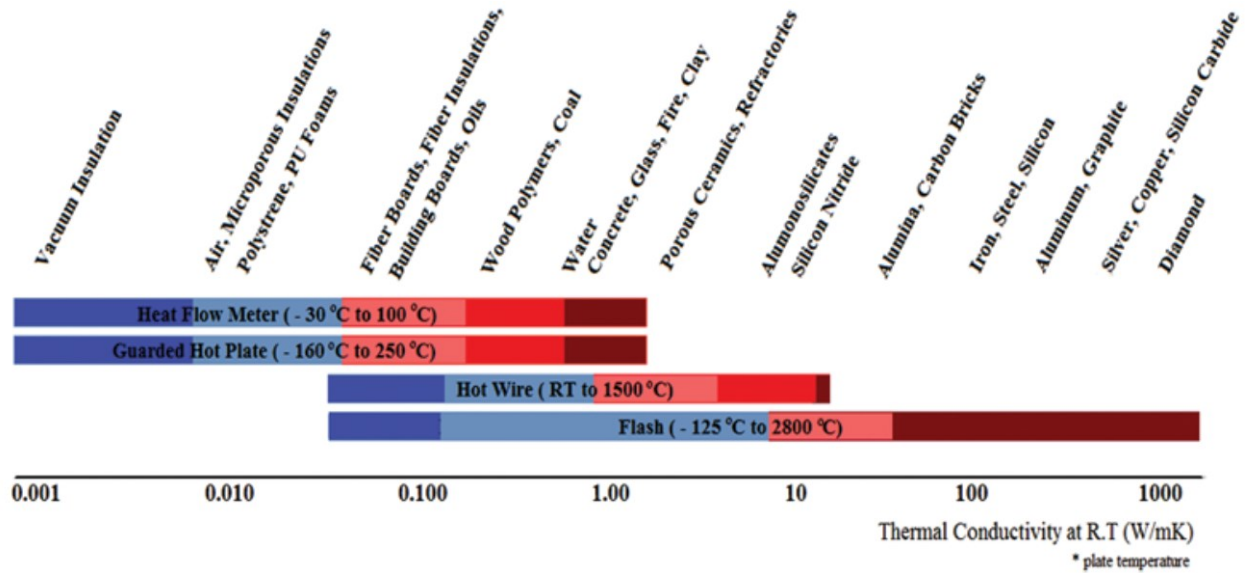
Figure 18: Comparison of measurement techniques and material type for range of thermal conductivity [58]
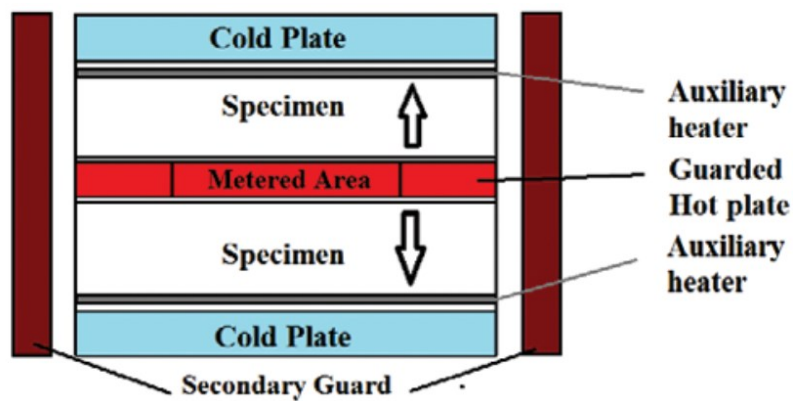
Figure 19: Schematic of the apparatus of the guarded hot plate method with two specimens [58]

Based on similar principles, a heat flow meter system, such as that schematically illustrated in Figure 20, provides faster results and is straightforward in operation. The basic concept behind this system is that the meter is determining heat flux based on a measured drop in

temperature through a thermally resistive specimen. This measurement is carried out by either using a well-known reference specimen, or a heat flux sensor, and the setup involves placing the test sample between two plates which are held at two different constant temperatures. When using heat flux transducers to measure the heat flow through the sample, the result is determined by measuring the voltage drop through an electrical resistor and this produces the output signal. This change in voltage is proportional to the drop in temperature occurring through the plate [58]. In contrast to the guarded hot plate which can be considered an absolute method, this result is comparative and can thus be considered a relative measure.
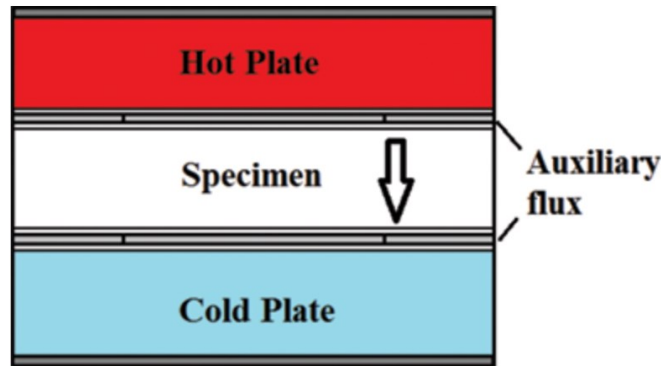
Figure 20: Basic schematic of heat flow meter setup [58]

The hot wire method is a transient technique based on recording the increase in temperature at a defined distance from a source of heat (Figure 21). This system is an effective means of determining the thermal conductivity of liquids as well as solids. For the former, the wire is placed between two specimens of equal size, each with small channels for the wires to reduce contact point resistance as much as possible. In this standard layout, the wire system serves as a heater and temperature sensor. The thermal conductivity in this method can be calculated by assessing the plot of the wire temperature vs time on a logarithmic scale, provided that the sample density and heat capacity are known. In materials that are amenable to it, the system can be modified such that a probe can be used to measure the temperature rather than a distinct wire from the heat source [58].
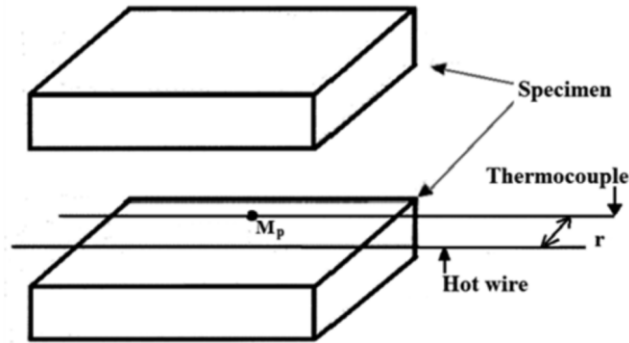
Figure 21: Basic schematic of parallel hot wire technique[58]

Laser flash analysis, LFA, is the most commonly used method for determining the thermal properties of solids – traditionally focused on the thermal diffusivity, α. With this measurement, and in combination with a known specific heat capacity and density for the material being tested, the thermal conductivity can be calculated with the following equation under adiabatic conditions [58], [59].

$$\alpha = \frac{k}{\rho c_p} \tag{6}$$

Where α is the thermal diffusivity of the material, k is the thermal conductivity, c_p is the specific heat capacity, and ρ is the density. The LFA system is functional in the determination of thermal diffusivity for a wide range of materials; from metals to glasses and ceramics. In addition to this, measurements can be conducted at temperatures ranging from -100°C to 3000°C, limited only the be temperature constraints of the given system.

In operation, an instantaneous heat pulse is applied to the sample with a laser. The temperature at the backside of the sample is then constantly measured until thermal equilibrium is re-achieved. At this point, the thermal diffusivity of the sample can be calculated based on the thickness of the sample and the time, as presented in the following equation (7):

$$\alpha = 0.138 \frac{d^2}{t_{\frac{1}{2}}} \tag{7}$$

Where,

α is the thermal diffusivity,

d is the thickness of the sample,

$t_{1/2}$ is the time to reach half-peak

The time value is representative of the time required for the back surface to reach half of its eventual maximum value. A number of models can be used both to plot the detector signal and track where this half-point is, at which a point final calculation can be completed.

Figure 22 presents a schematic illustration of a typical LFA system. The process was first developed in 1961 [59], and has received refinement in the subsequent years for improvements in accuracy and functionality [58], [60]. The LFA technique is advantageous as it does not involve temperature nor heat flow measurements to determine thermal properties, requiring only measurement of temperature change over time during laser shots. This allows for testing that is both fast, as well as accurate to within 3-5% range of uncertainty even at high temperatures [58]. One factor that can be observed to slow the LFA process though is testing at varied temperatures. For accurate readings, the baseline sample state must be extremely steady, as changes to that baseline are the basis of LFA measurement. Establishing this stable baseline at elevated temperatures is not trivial and can appreciably extend the measurement time required.
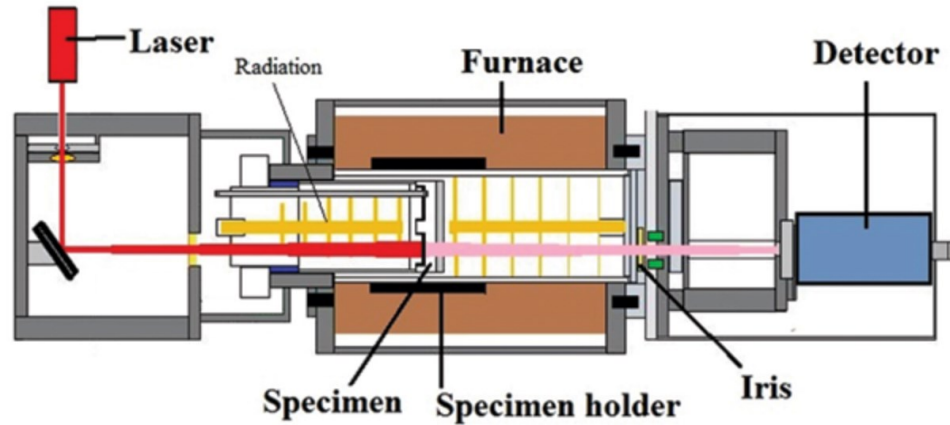
Figure 22: Schematic Diagram of LFA operation[58]

1.3.3 Thermal Expansion and Dilatometry

Thermal expansion is the tendency of matter to change shape/volume/density in response to changing temperature; typically in the absence of a phase change [61]. Thermal expansion is the result of complex changes at the scale of the atomic lattice. A commonly accepted theory suggests that the property is based on the increase in average distance between atoms with rising temperature. This transpires as increased temperature manifests increased extents of vibrational motion in the atoms. Such vibration is what is measured as temperature, but in addition to this, the atoms are not vibrating in unison. This results in an overall increase in the average spacing between the vibrating atoms [61]. It should also be noted that negative thermal expansion does exist [62], but focus will be maintained on the more frequently experienced positive expansion of materials.

The coefficient of thermal expansion is an experimentally determined characteristic of a material, quantified by through the change in dimension over the original dimension, vs. the change in temperature [63]. The coefficient of linear expansion can be described using the following equation (8):

$$\frac{\Delta L}{L_0} = \alpha \Delta T \qquad (8)$$

Where,

ΔL is the change in length,

L_0 is the initial length,

α is the coefficient of thermal expansion,

ΔT is the change in temperature

In a perfectly uniform lattice, thermal expansion will be 100% uniform in all directions, and even at the macroscopic scale it can usually be assumed that thermal expansion occurs uniformly. Figure 23 illustrates the relationship between the coefficient of linear, area, and volume expansion, and indicates how the later are x2 and x3 of the coefficient of linear expansion, respectively.
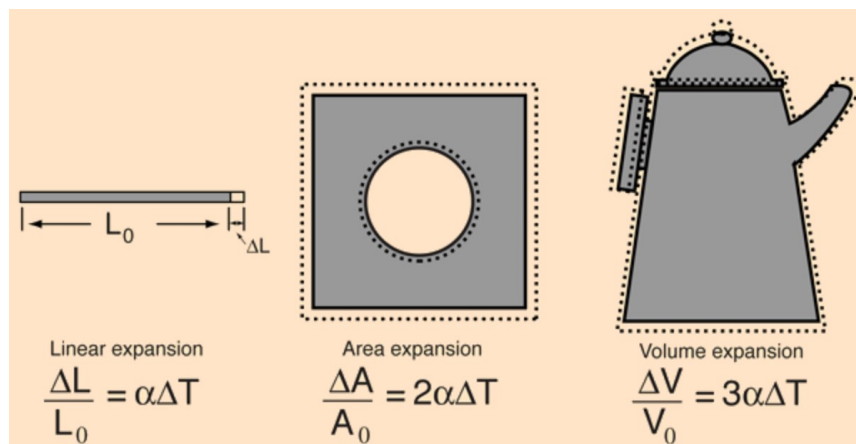
Figure 23: Coefficient of linear, area, and volume expansion relationship [63]

There are numerous factors that can influence the coefficient of thermal expansion for a material. Materials with properties leading to anisotropic thermal conductivity will also likely experience anisotropic thermal expansion. Lattice defects, such as interstitial atoms, vacancies, and boundaries can also impact the thermal expansion properties of a material. This also then leads into the impact of alloying additions, which can have a wide range of

impacts depending on the bulk matrix and solute addition, and their properties. Generally, it has been found that additions with a lower coefficient of thermal expansion than the bulk will result in an overall reduction in thermal expansion in the overall alloy system.

Thermal expansion, more specifically the coefficient of thermal expansion, is measured via dilatometry – the precise measure of volume or dimensional change in a given specimen. Classical dilatometry was conducted through the immersion of a sample in a fluid, historically mercury, and then measuring the volumetric expansion of the sample by constricting fluid in a capillary [64]. Modern dilatometry instead is based on the measure of linear expansion in one direction, utilizing the understanding that volumetric expansion is three times that of linear expansion.

Thermal dilatometry setups can vary, offering different ranges of functionality and cost. Some systems measure thermal expansion via contactless optical observation, while others utilize pushrod systems with the measuring rod in direct contact with the sample. Figure 24 outlines the layout of such a system, as well as the LVDT used to measure change in size of the sample.
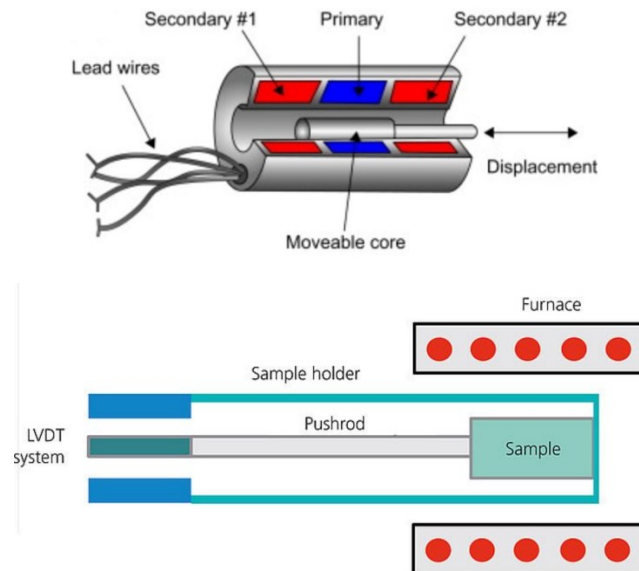
Figure 24: Schematic of LVDT [65] and pushrod-furnace testing chamber [66]

Pushrod dilatometers are the most common, and the main components of such a system are the Linear Variable Differential Transformer (LVDT), the pushrod, the furnace, and the thermocouple. The pushrod is connected to the ferromagnetic core of the LVDT at one end, and pushes against the sample at the other. As the sample changes in length the LVDT records this change as a voltage induced by the movement of the ferromagnetic core [62]. It is immensely important that the rod and surrounding apparatus are made from a material with a low coefficient of thermal expansion, and that any expansion can be very reliably account for and calibrated against. Fused silica or alumina are two materials that can serve this purpose. Sample preparation is also important, with accurate readings requiring absolutely parallel flat ends on the sample [66].

CHAPTER 2 – RESEARCH OBJECTIVES

The primary objective of this research is to expand the range of available aluminum alloys for PM manufacturing by developing new formulations that address strategic gaps in material performance in the sector. The specific alloy system targeted is a PM analogue to wrought aluminum alloy 6063 (Al-0.7Mg-0.5Si). This 6xxx alloy is relatively lean in Mg/Si contents which invokes exceptional thermal conductivity concurrent with a capacity for precipitation hardening. This development centers on minor chemical modification to enhance sinterability coupled with a rigorous exploration of each stage in the press-sinter-size production cycle to identify appropriate manufacturing parameters.

CHAPTER 3 – Powder Metallurgy Processing of an Al-07Mg-04Si-(Sn) Alloy

C.M. Spence[1], I.W. Donaldson[2], D.P. Bishop[1*]

1 – Dalhousie University, Department of Mechanical Engineering, 1360 Barrington Street, Halifax, NS, Canada, B3H 4R2
2 – GKN Sinter Metals, Advanced Engineering, 1670 Opdyke Court, Auburn Hills, MI, USA, 48326
*Corresponding Author: Paul.Bishop@dal.ca

Abstract

6xxx series (Al-Mg-Si) alloys represent one of the most widely used systems for automotive applications, offering an advantageous balance of thermal conductivity, formability, and strength. In a wrought context, over 45 unique 6xxx alloy chemistries are available to end-users yet in the powder metallurgy (PM) sector there is but one (PM6061). To address this shortcoming, research in this project seeks to devise PM systems that are lean in Mg/Si contents so as to invoke maximum thermal conductivity. Chemistries comparable to wrought alloy 6063 (Al-0.7Mg-0.5Si) were investigated for this purpose using commercially available powders. The response of this material to press-and-sinter processing was studied with an emphasis on ascertaining the effects of small additions of tin, and variations in key PM processing parameters (compaction pressure, sintering temperature/time). Metallurgical characterization of the sintered product included microstructural analyses, density measurements, thermal diffusivity testing, and mechanical testing. Select formulations achieved >99% theoretical density and thermal conductivities that closely matched those of the wrought equivalent.

Keywords: Aluminum powder metallurgy, 6063, sintering, thermal properties

3.1 Introduction

Aluminum is the second most utilized metal in the world, behind only iron. The wide and varied usage of this metal is attributed to a combination of material properties that allow it to fill a broad range of applications. For example, aluminum is light weight, while certain aluminum alloys have excellent strength yet maintain a relatively low density that manifests a high strength to weight ratio. Others exhibit good electrical and thermal conductivity, and many are corrosion-resistant in prescribed environments. In addition, the production of engineered components from aluminum alloys is feasible using a variety of metal working technologies including casting, forging, extrusion, and more recently, powder metallurgy (PM) [30].

The development of aluminum PM processes has been ongoing for some time, but commercially viable options did not come about until well after PM processing was well established for a range of other metals (ferrous, copper, etc.). In the past thirty years the PM processing of aluminum alloy powders has expanded greatly however, both in available chemistries and in the scope of commercially viable applications [1], [4]. The first large scale commercially utilized PM aluminum alloy chemistry was established in 1992 as a counterpart of the wrought alloy 2014. In the ensuing years, a number of other alloy compositions have emerged [4]. Typically, these have come by adapting wrought chemistries such that they can be viably used in a PM context. Examples of successful PM counterparts to wrought aluminum alloys include variants of 2014 [28], [67], as well as 2024 [8], [68], 2618 [69], 7075 [8], [29], [70], 4032 [7], and 6061 [14], [15], [71], [72]. Notably, the latter is, at present, the only commercially utilized 6xxx series aluminum alloy in the high volume press-and-sinter PM sector.

6xxx series alloys are based around the Al-Mg-Si system. There are many unique alloy chemistries within this specific series involving prescribed ranges in magnesium and silicon contents as well as a number of minor additions such as copper, chromium, and manganese [47]. 6061 is the most utilized system, as it offers a high strength in combination with good extrudability, ease of manufacture, and adequate corrosion resistance for many scenarios. Another notable entry of the 6xxx series is 6063; a lean alloy with a typical

chemistry of Al-0.7Mg-0.4Si [47]. This particular system is popular in end use applications wherein a heightened thermal conductivity is required in combination with good extrudability and moderate strength [38], [47], [73]. This balance of properties makes it a popular choice for components such as heat sinks that are of growing commercial importance in several sectors such as electrified vehicles. To this end, the objective of this research was to develop a PM counterpart to wrought aluminum 6063 that maintains a comparable balance of thermal and mechanical properties but is also amenable to a high-volume PM production environment.

3.2 Materials

The base alloy in all instances was a PM counterpart to wrought 6063 and targeted a nominal chemistry of Al-0.7Si-0.4Mg-xSn (weight %). In all instances, the principal powdered material was air atomized elemental aluminum powder ($D_{50} = 116\mu m$). Silicon was sourced as a gas atomized 88Al-12Si (weight %) master alloy powder ($D_{50} = 33\mu m$) whereas tin was sourced as a gas atomized elemental powder ($D_{50} = 4\mu m$). All three powders were produced by Kymera International. Magnesium was sourced as an elemental, inert gas atomized powder ($D_{50} = 31\mu m$) produced by Tangshan Weihao Magnesium Powder Company Limited. Each blend also included 1.5 weight % of a powdered wax (LicoWax C; Clariant Corporation) for the purposes of tooling lubrication during die compaction. Tin concentrations of 0, 0.25, 0.50, and 1.0 weight % were investigated to assess its potential for the enhancement of sintering-induced densification. Designations for the four alloy chemistries considered are thereby based on the respective tin concentration and are hereafter annotated as 0.0Sn, 0.25Sn, 0.5Sn, and 1.0Sn. For comparison purposes, rods of extruded wrought 6063-T5 were procured and assessed as well.

3.3 Experimental Techniques

PM samples were produced through a combination of powder blending, uniaxial die compaction, sintering, and post-sinter sizing. Starting powder blends were prepared by mixing the required combination of powders in a Turbula model T2M mixer in three stages. Each stage involved a mixing time of 35 minutes. First, the aluminum and aluminum-silicon master alloy powders were combined. This was followed by magnesium and tin additions with the powder lubricant added last. Blends were then die compacted using an Instron Satec test frame (model 5594-200HVL) equipped with a 1 MN load cell and a floating die tooling assembly at pressures ranging from 150 to 550 MPa. Transverse rupture strength (TRS) bars (32.5 x 12.5 x 10mm) and charpy bars (75 x 12.5 x 12.5mm) were compacted for the assessment of general sintering response and tensile properties respectively. Compacted specimens were sintered in a Thermo Scientific Lindberg/Blue M Model STF55666C-1 tube furnace under flowing high purity (99.999%) nitrogen atmosphere. All sintering profiles included a 20 minute hold at 400°C for de-lubrication purposes, followed by a ramp to the required sintering temperature (610°C to 640°C) where specimen were isothermally held for 5 to 30 minutes prior to cooling. Sizing was applied to sintered bars at pressures ranging from 100 MPa to 400 MPa using the same Instron test fame and tooling.

Sintered densities were determined via MPIF standard 42 [74] using a Sartorius YDK03 balance coupled with a density determination kit and oil infiltration. Hardness testing was conducted with a Wilson Instruments RB2000 Rockwell hardness tester in the HRE hardness scale. Prior to hardness testing each specimen was lightly ground with a Buehler MetaServ manual Grinder-Polisher with 400 grit SiC and continuous water flow. Tensile testing was conducted using the aforementioned test frame but when equipped with a 50 kN load cell and an Epsilon model 3542 axial extensometer. Samples were machined to cylindrical threaded tensile bar specifications compliant with ASTM E8M [75] including a gauge section that was 30mm long and 6 mm in diameter. Each sample was loaded at a rate of 5MPa/s and the extensometer remained attached through to the point of fracture. Microstructural Analysis was conducted using a Keyence Profile-Analyzing Laser

Confocal Microscope, VK-X1000 series. In all instances, samples were mounted in bakelite and then ground/polished through a series of stages with silicon carbide papers, diamonds pastes, and colloidal silica. All imaging was conducted with a coaxially aligned light source and optical camera mode of operation.

Thermal dilatometry, differential scanning calorimetry (DSC), and thermal diffusivity tests were also completed. PM specimens needed for these purposes were machined from the center of sintered TRS bars and then cleaned with petroleum ether prior to testing. For dilatometry, machined cylindrical samples 25mm in length and 6mm in diameter were prepared and then tested in a Netzsch 402C pushrod dilatometer. Temperature calibration was completed by melting small quantities of high purity Sn, Zn, and Ag between alumina disks and comparing the known melting temperature to that at which thermal expansion showed an abrupt drop. Displacement calibration was achieved by measuring the thermal expansion of a single crystal of sapphire and then comparing measured and known values. This test was then repeated with a specimen of high purity aluminum with dimensions identical to the samples being analyzed. Each sample was heated at 5 K/minute to 350°C in an air atmosphere.

For DSC, cylindrical samples 4mm in diameter and 1mm in length were placed in pure alumina crucibles and tested in a Netzsch DSC 404 F1 under a static argon flow (50 mL/min). A heating rate of 10 K/min was applied with a 20 minute hold at 40°C to ensure thermal equilibrium before continued heating to a maximum temperature of 590°C. For each specimen, three runs were required to determine specific heat capacity (Cp) using the ratio method in accordance with ASTM standard E1269 [52]. First, a baseline correction curve was produced by running the test program with an empty crucible. A second run was then completed with a sapphire standard of known Cp. In the third and final run, the actual specimen was tested.

Thermal diffusivity samples were polished plates (10mm x 10mm x 3mm) coated with a thin layer of graphite to minimize surface reflectivity. These were tested in a Netzsch 427 Laser Flash Apparatus (LFA) under a flowing argon atmosphere (150 mL/min). Key parameters included a heating rate of 20 K/min, a minimum temperature stability threshold

of 0.5 K/30s to ensure an accurate temperature value for each reading, a laser voltage of 550V, and a pulse width of 0.30ms. Five readings were taken at ambient (~23°C), 50°C, 100°C, 150°C, 200°C, and 250°C. For each, an adiabatic – pulse correction model was utilized by the Proteus LFA analysis software to identify the half-rise time and covert it to a thermal diffusivity value.

3.4 Results and Discussion

3.4.1 Sintering Behaviour

3.4.1.1 General Sintering Response

The first stage in determining the viability of the 6063 PM systems was an examination of the general sintering behaviour of each chemistry. Three of the four alloys considered contained a controlled amount of tin. This element is not a standard feature of wrought 6063, however it is known to perform as an effective sintering aid and a catalyst for densification in aluminum PM alloys [1]. Hence, it was included as a potential benefactor within this otherwise lean alloy chemistry. Initially, samples of each chemistry were compacted and sintered at increasingly higher temperatures. A fixed compaction pressure (250 MPa) and sintering hold time (20 minutes) were utilized in all instances based on prior work with other PM systems [14], [71].

The final densities for each alloy chemistry were tracked for sintering temperatures of 610 to 640°C (Figure 25). The 0.0Sn systems exhibited poor densification across the entire temperature range with only a modest improvement noted at 640°C. The peak value was <96% of full theoretical and thereby fell well below the level routinely achieved in other aluminum PM systems [69], [8], [29], [70]. The value of the tin additions was obvious, confirming that a direct translation of wrought chemistry does not necessarily lead to reasonable densification in PM processing. All tin-containing chemistries saw initial improvement in densification with increasing temperature. The 0.25Sn and 0.5Sn systems maintained a gradual improvement through to 630°C at which point no further gains or degradation were noted. The 1.0Sn alloy also improved with rising sintering temperature

but density plateaued at a slightly lower temperature of 620°C. All three tin-laden chemistries densified similarly in the 630 to 640°C range wherein peak final densities were all in the general vicinity of 98.5 to 99% of full theoretical. Sintering runs at temperatures >640°C were deemed unnecessary as the propensity for distortion became excessive to a point where such processes would be ineffective in an industrial production setting.
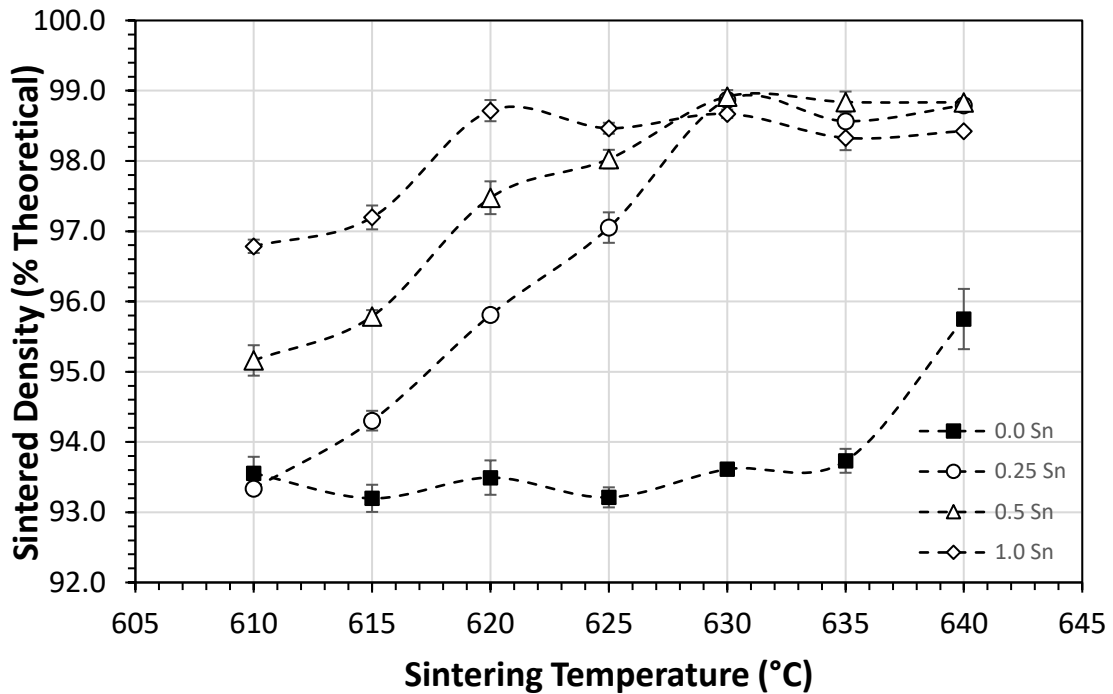
Figure 25: Sintered density versus sintering temperature for the PM chemistries considered.

The mass change incurred as a result of sintering was also tracked as shown in Figure 26. All tin-containing systems exhibited a net mass reduction of ~1.5 weight %. This was consistent with the concentration of the wax lubricant utilized and inferred that the delubrication stage of the sintering cycles was effective. Net mass loss from the 0.0Sn system was in stark contrast. Here, inferior changes that varied from ~1.15% to ~1.35% and trended downward from low to high sintering temperatures were measured. As all samples were sintered concurrently and through a common thermal stage for delubrication

(400°C for 20 minutes) incomplete delubrication was ruled out as a contributing factor in mass losses for 0.0Sn. The root cause was believed to stem from a heightened propensity for in-situ nitridation. In this sense, when Al-Mg PM alloys are sintered, the Mg invokes a fluxing effect on powder particle surfaces to expose metallic aluminum. This feature will then readily react with gaseous N_2 to invoke nitridation and a concomitant mass gain [24]. As such, the net mass losses will then fall short of the concentration of admixed lubricant powder even though the entirety of this blend constituent has been removed. The nitridation reaction is reduced appreciably in the presense of tin [13], [24]. Tin melts early in the sintering cycle (232°C) and spreads over the powder particles to thereby limit their direct exposure to the sintering atmosphere. This throttles back the extent of nitridation such that the net mass change becomes nominally equivalent to the total concentration of admixed lubricant powder.
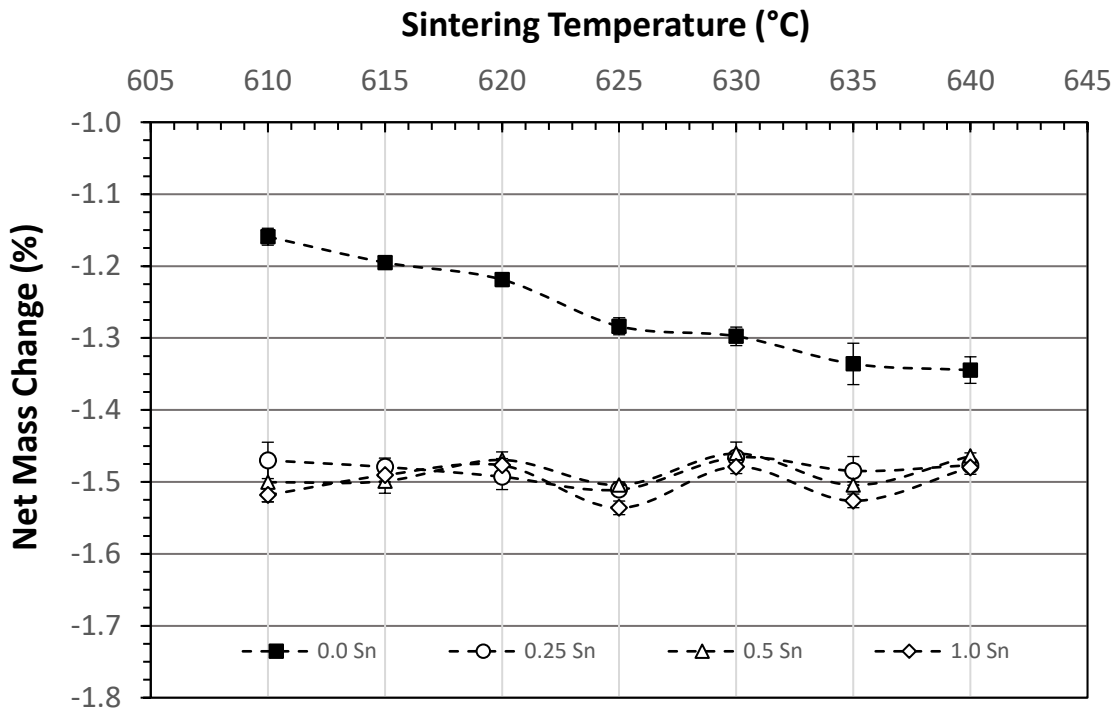
Figure 26: Mass Change During Sintering vs. Temperature for all PM chemistries

Hardness data for the alloys after sintering at the temperatures considered are presented in Table 2. The trend for each alloy tracked reasonably well with sintered density, as would logically occur when comparing samples with significantly different levels of residual porosity. The 0.0Sn alloy exhibited a relatively low hardness across the range of sintering temperatures wherein an effectively static sintered density of 93.5% was measured. Hardness then improved at 640°C in keeping with the slight density increase. The nominal hardness for 0.25Sn and 0.5Sn were quite consistent and similar when sintered between 625 to 640°C. Values in this range were generally 10-15 points higher than the 0.0Sn counterpart. The 1.0Sn system had a consistently lower hardness than the other two Sn-bearing alloys. Densities were slightly lower in this alloy and had likely contributed to this observation. However, it was also conceivable that the higher level of Sn had scavenged a greater portion of the Mg present. These elements are known to react to form Mg_2Sn during sintering cycles [10]. Preferential reaction to form this stable intermetallic would have then deprived the α-Al grains of Mg and thereby lessened the capacity to form β-type (Mg_2Si) precipitates which are known to be the key strengthening feature of wrought 6063.

Table 2: Hardness of PM specimen sintered at various temperatures.

Sintering Temp. (°C)	Hardness (HRE)						
	610	615	620	625	630	635	640
0.0Sn	18±5	15±3	16±4	13±2	15±3	16±5	25±1
0.25Sn	5±3	14±5	18±12	25±7	29±6	30±7	30±7
0.5Sn	10±6	19±7	23±7	23±8	25±9	25±8	24±10
1.0Sn	11±5	12±6	11±4	17±7	12±9	20±9	18±3

The final metric evaluated in this initial analysis of sintering response was the net amount of dimensional change instilled because of sintering. Figure 27 presents the percentage change in specimen width across the temperature range considered. This trait tracked closely to an inversion of the densification response. The elimination of porosity during

sintering leads to an increase in density, but also a reduction in overall volume. This is then manifested as a negative value for dimensional change. The 0.0Sn chemistry did not present any appreciable shrinkage until 640°C, consistent with a general absence of meaningful densification. Sn-bearing alloys had shrunk over all sintering temperatures but the net effect became somewhat static when sintering at ~630°C and higher. Peak values were in the range of 2% shrinkage which is typical for alloys of this nature. Based on the combined data on sintered density, hardness, and dimensional change, a common sintering temperature of 635°C was utilized in subsequent studies. This selection was based primarily around the resultant characteristics of the tin-containing chemistries, as the 0.0Sn alloy demonstrated poor results across every metric regardless of temperature.
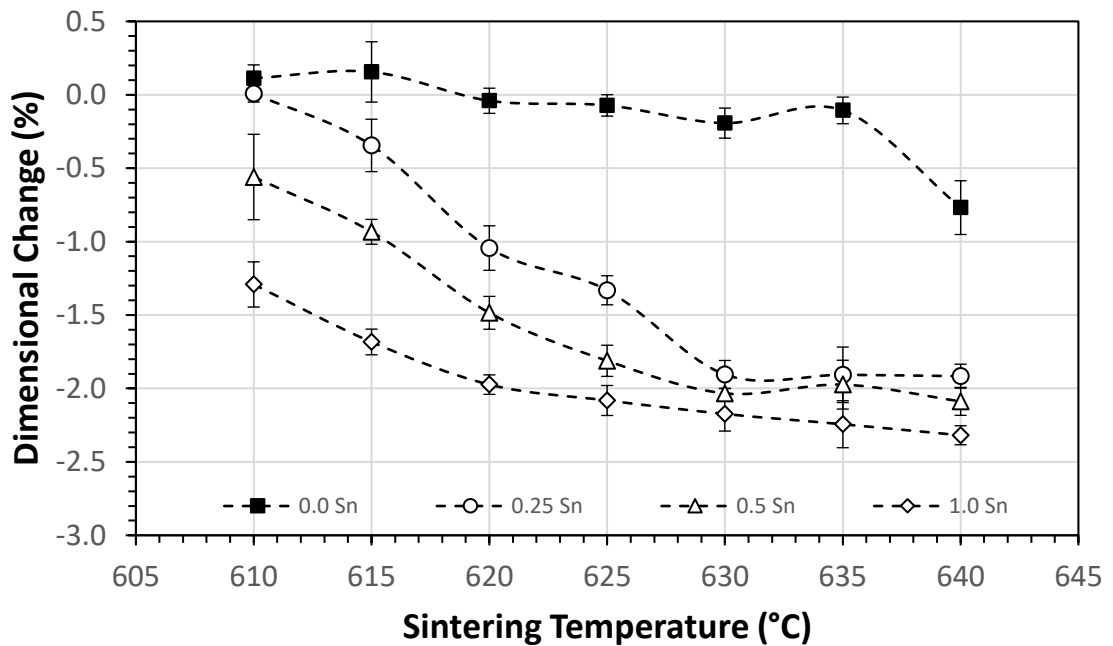
Figure 27: Dimensional change as a function of sintering temperature.

3.4.1.2 Effects of Compaction Pressure

The determination of an appropriate sintering temperature for the tin-containing chemistries still left room for further improvement in densification response through the modification of additional processing parameters. In this context, the role of the compaction pressure utilized to fabricate green compacts was considered and was varied over a range typical of the values implemented in commercial PM operations (150 to 550 MPa). For this stage of analysis, all sintering parameters were fixed. Namely, a 20 minute hold at a sintering temperature of 635°C. Data illustrating the effect of compaction pressure on sintered density are presented in Figure 28. As with the examination of sintering temperature, the densification response of the tin-containing chemistries again differed significantly from that of the 0.0Sn alloy. For the former, compaction pressures of 250 MPa and greater offered no significant change in densification response. A pressure of 150 MPa manifested a slightly lower sintered density, but was still quite effective in an overall sense. However, for the 0.0Sn chemistry, compaction pressure had a statistically meaningful impact at values <350MPa. Above this point, sintered density remained static at ~95% of theoretical. This analysis indicated that compaction pressure had minimal influence on the densification response of PM chemistries that incorporated a tin sintering aid. The same could not be said for the 0.0Sn system and it is also apparent that increased compaction pressure could not resolve its inferior sintering response.
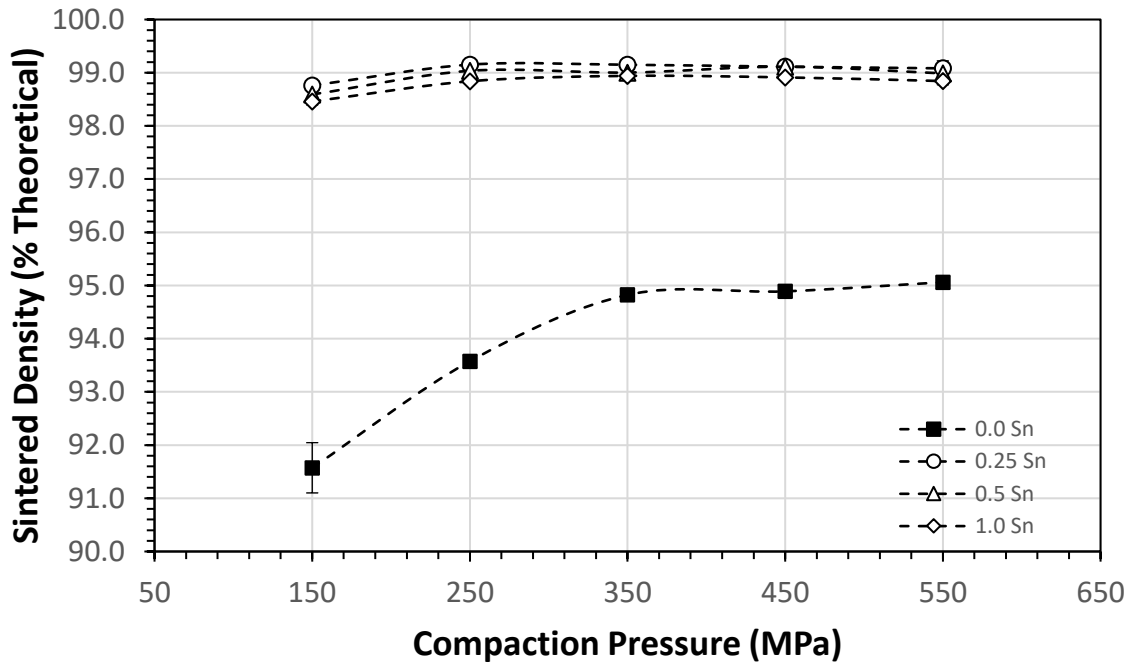
Figure 28: Effects of compaction pressure on the sintered density of the PM alloys investigated.

As shown in Table 3, compaction pressure did not have a statistically significant impact on the hardness of any of the tin-containing chemistries, and while there was very minor improvement for 0.0Sn between 150 and 250 MPa, no further changes of significance occurred. However, it was found to influence the dimensional change characteristics of the test specimen (Figure 29). The extent of which was pronounced at pressures of 150 to 250 MPa but then became much more subtle at higher pressures. Evidently, while the presence of a sintering aid allows these systems to effectively densify, the substantively lower initial green density from the lower compaction pressures requires more material movement to reduce internal porosity. This was also true for the 0.0Sn system, though the magnitude of improvement with increasing pressure was appreciably smaller.

Table 3: Effects of compaction pressure on the hardness of sintered PM products.

PM Alloy	Hardness (HRE)				
	150 MPa	250 MPa	350 MPa	450 MPa	550 MPa
0.0Sn	10 ± 3	17 ± 6	18 ± 3	20 ± 6	20 ± 3
0.25Sn	31 ± 2	32 ± 5	30 ± 5	30 ± 4	25 ± 7
0.5Sn	39 ± 2	38 ± 3	36 ± 3	35 ± 4	35 ± 4
1.0Sn	30 ± 4	33 ± 2	33 ± 2	34 ± 2	33 ± 3
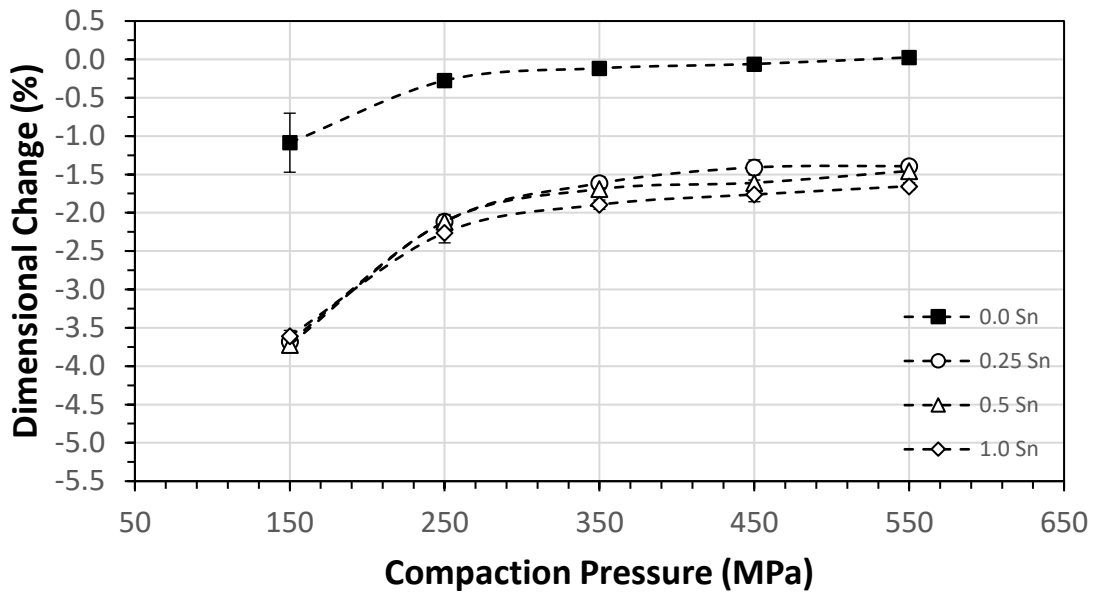
Figure 29: Effect of compaction pressure on the sintering-induced dimensional change of PM compacts.

As with sintering temperature, an effective compaction pressure was identified through the consideration of its impact on densification, hardness, and dimensional change. Primary consideration was again focused on the tin-containing systems due to their superior performance. Based on this analysis, a pressure of 350 MPa was selected for the subsequent production of test specimen.

3.4.1.3 Effects of Sintering Time

A final fundamental parameter for determining the general sintering behaviour of the PM chemistries was sintering time. While sintering times of 20 to 30 minutes are typical for many aluminum PM alloys [1], [4], it is valuable to ascertain a range of viable sintering times just as with sintering temperature and compaction pressure. For this analysis, sintering times from 5 to 30 minutes were used, in conjunction with a fixed compaction pressure (350 MPa) and sintering temperature (635°C). As can be seen in Figure 30, sintering time had a relatively minor impact. Across all four chemistry variants, subtle gains were noted as sintering time was increased from 5 to 20 minutes with no significant improvements noted beyond this point. Hardness likewise exhibited minimal impact from sintering time as there was no statistically significant change in this trait for any of the four chemistries across the entire range of sintering times. Similarly, dimensional change did not see any impact from sintering time, remaining consistent from 5 minutes through to 30 minutes for all four chemistries. These findings confirmed that a 20 minute hold time was reasonable for the alloys. They also indicated that an extended sintering period was ineffective at resolving the recurrent challenges associated with the 0.0Sn system.
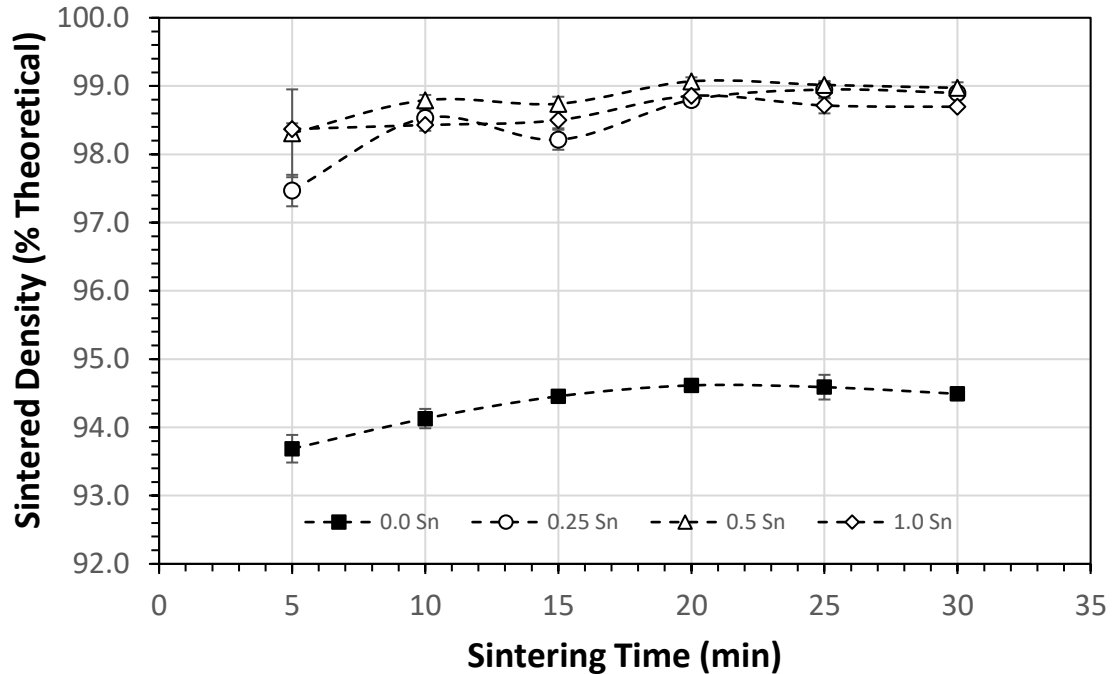
Figure 30: Effects of sintering time on the sintered density of PM compacts.

3.4.2 Post-Sinter Sizing

While it is necessary to identify appropriate parameters for the sintering process, as-sintered specimen are not fully representative of those produced industrially as these are invariably subjected to a post-sintering sizing operation. Here, sintered blanks are cold formed in rigid tooling under high load to refine dimensional tolerances, eliminate sintering-induced distortion, and enhance mechanical/physical properties; after which, the product is then allowed to naturally age to an effectively stable hardness before utilizing it in service. This sequence is akin to a T2 tempered state in the context of wrought aluminum metallurgy and this nomenclature has since been adopted in commercial PM practice. As such, the effects of sizing were investigated to enhance the industrial relevance of the study.

Work in this area began by monitoring the sintered samples for any change in hardness with time after sintering. Data of this type are essential as sintered aluminum PM alloys, that are precipitation hardenable, are known to exhibit natural age hardening [28]. As such,

61

the formability of the material can change with time which influences critical factors such as the load required for sizing and the propensity for sizing-induced cracking. For this situation, post-sinter aging curves were developed for the 0.25Sn and 0.5Sn systems, as they showed the most promise for peak material properties based on the analysis of general sintering behaviour. Each aging curve was developed through hardness measurements of sintered bars over a range of post-sinter times that spanned from 30 minutes to 30 days. The resultant curves are displayed in Figure 31. In both instances, significant changes in hardness eventually transpired. The increases were minimal within the first 24 hours but soon thereafter an obvious rise was observed. The onset of significant hardening for 0.25Sn began between aging times of 24 and 96 hours (1 to 4 days). Conversely, that for 0.5Sn was delayed until aging between 96 and 216 hours (4 to 9 days). Both chemistries reached the better part of their peak aged state by the 9 day mark with minimal gains thereafter. The natural aging curves aided in the development of effective processing parameters that would yield samples in a T2 state. This particular temper designation is a PM industry standard and requires that products be cooled from the fabrication temperature, cold worked, and then naturally aged. Therefore, all sizing operations on as-sintered samples were conducted precisely one hour after sintering. This facilitated specimen consistency and concomitantly ensured that the sizing operation was carried out before any significant degree of natural aging could occur.
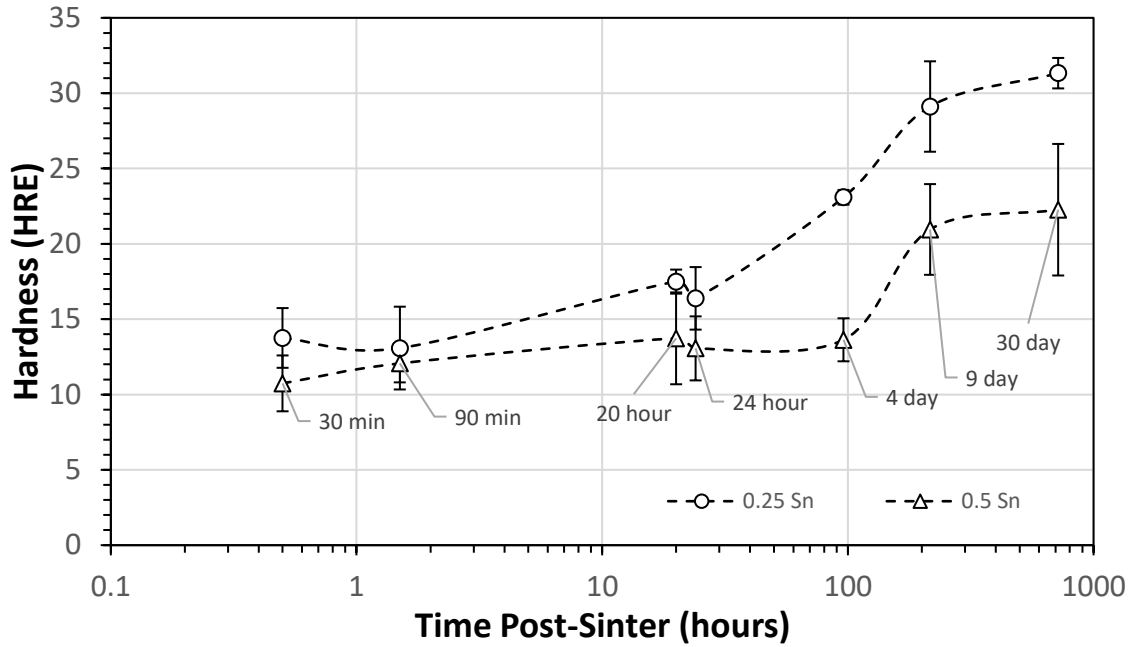
Figure 31: Post-sinter aging curves for 0.25Sn and 0.5Sn alloys. All samples aged under ambient laboratory conditions (~20°C).

Next, the effects of sizing pressure were considered. Data on the impact of this parameter are shown in Table 4. Results confirmed that sizing was an effective means of improving the final density and hardness of the 0.25Sn and 0.5Sn systems. The gains were greatest in both alloys at the highest pressure considered (400MPa). Net density increases were relatively minor (~0.2 to 0.4%) but were statistically significant. Those for hardness were more apparent as the average hardness rose by 17 and 18 points for 0.25Sn and 0.5Sn respectively.

Table 4: Effects of sizing pressure on the sized density and hardness of PM specimen. All samples aged for 30 days after sizing.

| Attribute | Alloy | Sizing Pressure (MPa) | | | | |
		0	100	200	300	400
Sized Density (% Theoretical)	0.25Sn	98.8 ± 0.04	98.9 ± 0.04	99.0 ± 0.05	99.2 ± 0.05	99.3 ± 0.01
	0.50 Sn	99.0 ± 0.05	99.0 ± 0.04	99.1 ± 0.03	99.1 ± 0.07	99.2 ± 0.04
Hardness (HRE)	0.25Sn	27 ± 4	33 ± 5	37 ± 4	41 ± 5	44 ± 4
	0.50 Sn	22 ± 6	33 ± 8	36 ± 8	37 ± 6	40 ± 5

For future stages of analysis, consistency in sizing was important. However, due to the lack of appreciable shrinkage during sintering for the 0.0Sn system, the samples produced for this system could not fit into the sizing die utilized for Sn-bearing systems. Hence, they needed to be sized in an unconstrained manner within a larger die. Without the intended dimensional constraints, sizing deformation could result in excessive horizontal material displacement and barrelling of the sample if sizing was carried out at the same pressure for both the constrained and unconstrained die. Therefore, a target sizing reduction of 3.5% in height was implemented instead, based on the reduction of the tin-bearing systems when sized in the constrained die at 300 MPa. Through trial it was found that to match this reduction as closely as possible in the unconstrained die, a compaction pressure of only 120 MPa would be required. While this inconsistency for the 0.0Sn system was not ideal, it was deemed worthwhile to ensure the more promising alloy systems could be sized under conditions that matched industrial conventions as closely as possible, thus the use of a constrained die was maintained for the other three systems.

Figure 32 (a-d) presents optical micrographs of each of the four alloy systems in the T2 state. In line with the results of initial analysis, the porosity was very consistent across the three tin-bearing chemistries (Figure 32 (b-d)), further corroborating the significant benefit to sintering response brought on by the tin additions. The significant porosity of the 0.0Sn chemistry (Figure 32 (a)) confirms the reduced densification capability of the system, and how sizing was ineffective at eliminating residual porosity to any significant extent.

(a)

(b)

65
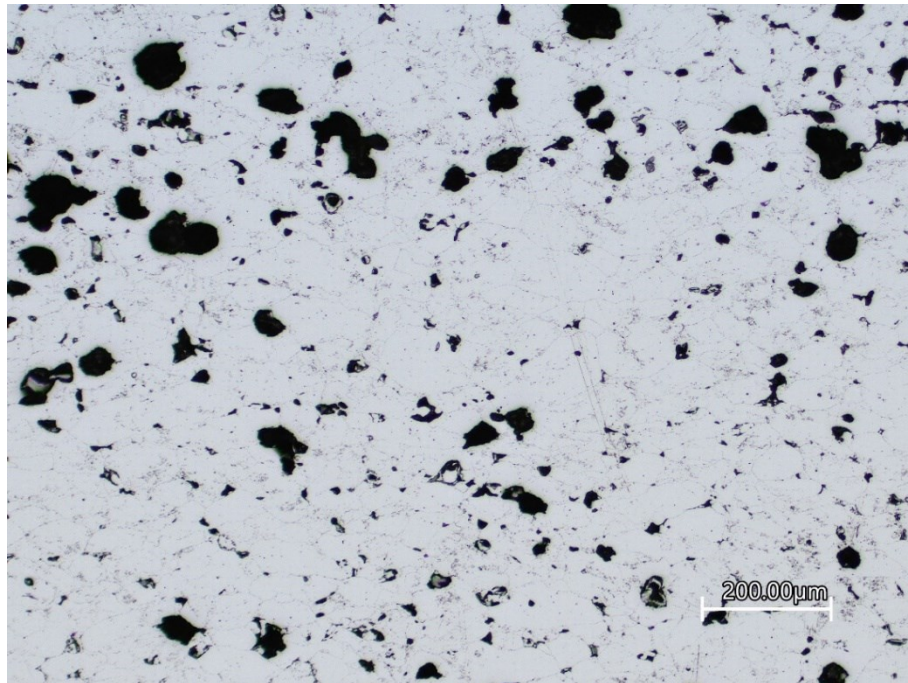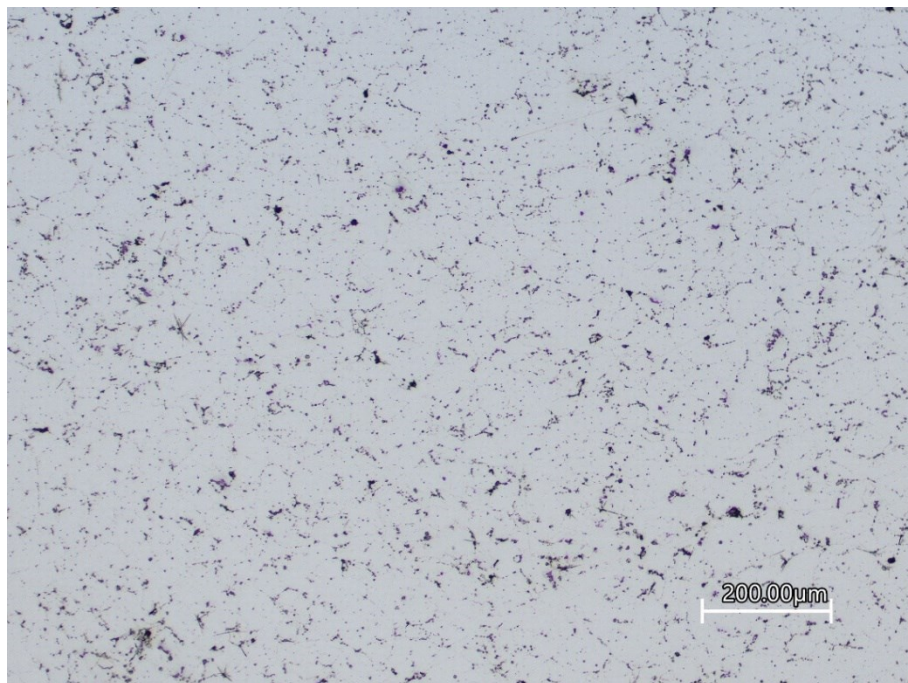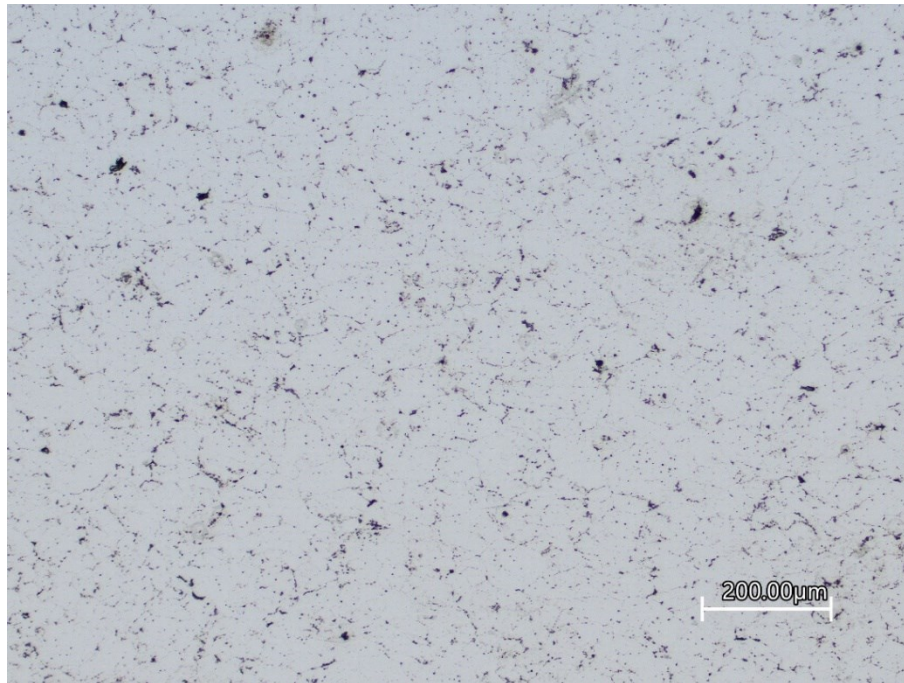
(c)
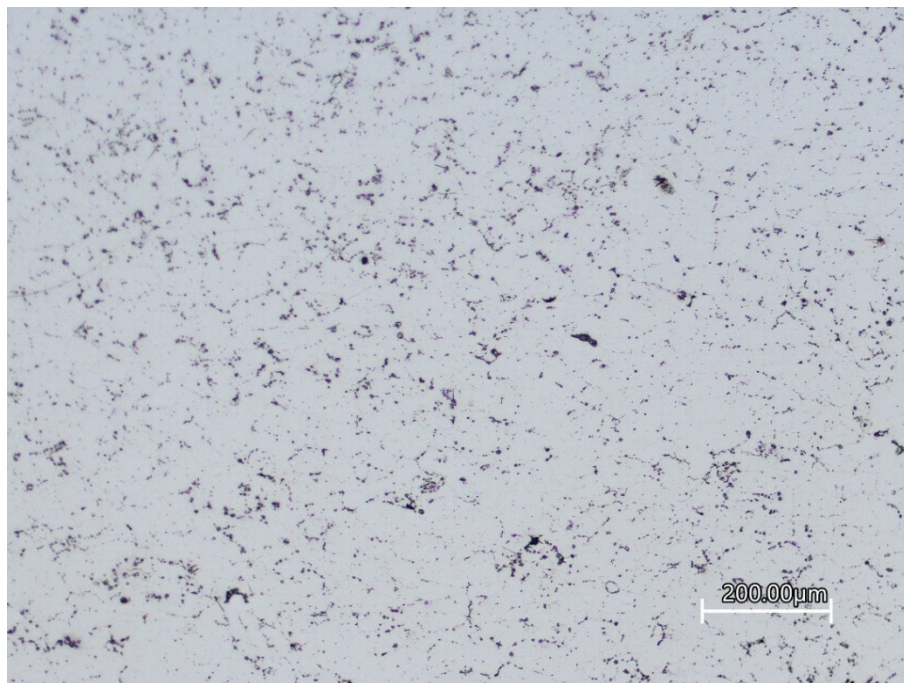
(d)

Figure 32: Optical micrographs of the four PM chemistries in the T2 state, (a) 0.0Sn, (b) 0.25Sn, (c) 0.5Sn, (d) 1.0Sn.

3.4.3 Tensile Property Assessment

Tensile properties of the PM alloy variants were measured for samples that had been processed through the complete T2 cycle of compaction, sintering, sizing, and natural age hardening. The resultant data are shown in Table 5. Not surprisingly, the inherently higher volume fraction of porosity in 0.0Sn samples manifested inferior tensile properties. This was particularly acute when considering the elongation to fracture as the average value was 6 to 7 times less than those measured for Sn-bearing counterparts. This highlighted the strong dependency of porosity on this trait. Statistically equivalent values for all tensile properties were measured for the remaining PM systems regardless of the net tin content. Those for yield strength and UTS fell short of the wrought benchmark. However, ductilities were quite exceptional for a PM alloy in the T2 state and were well aligned with the wrought system. This was viewed as a promising outcome for these PM materials as wrought-like ductility is rarely observed and typically mandates more aggressive post-sinter operations such as hot forging [76].

Table 5: Tensile properties for PM alloys in the T2 state. Typical data for wrought 6063-T5 included for comparison purposes [47].

Alloy	E (GPa)	Yield Strength (MPa)	UTS (MPa)	Elongation (%)
0.0Sn	59 ± 6	89 ± 1	105 ± 8	2 ± 1
0.25Sn	67 ± 6	94 ± 5	128 ± 8	12 ± 3
0.5Sn	75 ± 6	99 ± 1	134 ± 2	15 ± 3
1.0Sn	64 ± 11	102 ± 2	131 ± 2	15 ± 2
6063-T5	*68.3*	*145*	*186*	*12*

3.4.4 Thermal Analysis

Wrought 6063 exhibits excellent thermal conductivity and is frequently utilized in the fabrication of heat dissipation devices. As such, a PM counterpart to this material could be deployed in similar applications if it also demonstrated appropriate thermal properties. To this end, a comprehensive evaluation of the thermal conductivity of the PM systems was an important endeavor. Doing so requires knowledge of three key properties - the coefficient of thermal expansion (CTE), the thermal diffusivity (α), and the specific heat capacity (c_p). These values can be used together in the following equation (9) to calculate the thermal conductivity of a material at a discrete temperature:

$$k = \alpha \rho c_p \tag{9}$$

Where,

k = thermal conductivity

α = thermal diffusivity

c_p = specific heat capacity

ρ = density

The thermal diffusivity and specific heat capacity are used directly in this calculation. The CTE on the other hand is vitally important for use as a correction factor in other parts of the analysis. The determination of thermal diffusivity relies on a precise measure of a sample's thickness, and as testing temperature rises the thermal expansion of the sample must be accounted for. Similarly, correction for volumetric expansion is required for the determination of thermal conductivity at elevated temperatures.

Initially, data on the CTE were acquired over a range of temperature intervals (Table 6). The specific temperature ranges listed in Table 6 correspond with the those subsequently targeted for thermal conductivity determination. However, values for any temperature within then total test range can be easily determined as well given the continuous nature of

data collection. Regardless of alloy system, and indeed regardless of PM or wrought processing, the CTEs for all samples were consistent. This indicated that the additions of tin as well as any differences in the respective densities of the PM materials had minimal impact on this material property.

Table 6: CTE values measured for PM specimen in the T2 state. Data acquired from wrought 6063-T5 included for comparison purposes.

Temperature Range (°C)	CTE ($\mu m \cdot m^{-1} K^{-1}$)				
	PM System				Wrought
	0.0Sn	0.25Sn	0.5Sn	1.0Sn	6063-T5
20-100	23.33	23.45	23.42	23.16	23.40
20-150	24.03	24.34	24.34	24.06	24.18
20-200	24.72	25.12	25.20	24.84	24.96
20-250	25.14	25.74	25.83	25.50	25.22

Determination of specific heat capacity (c_p) via DSC is an involved process, but careful, repeated testing can provide accurate values over ranges of elevated temperatures. A primary limitation of this method is the inherent requirement for DSC analysis to establish thermal stability at the beginning of a test. This is normally unimportant for most DSC applications, but in the case of c_p determination, it meant that accurate c_p determination could only occur at temperatures in excess of 100°C. Thermal stability above 100°C is only one limitation on usable portions of data however. At more elevated temperatures, the prevalence of thermal events within the material impedes analysis, as the thermal energy entering the system no longer directly correlates only to temperature increase. The occurrence of these thermal events begins at approximately 220°C, and continued instability beyond that point disallowed for further accurate c_p determination. Due to these limitations, confidence in the values determined for c_p is constrained to this region of 100-

220°C, and Table 7 lists the c_p values of target temperatures within this range that could be used for further analysis in the determination of thermal conductivity.

Table 7: Measured heat capacities at target temperatures for PM specimens in the T2 state. Data acquired from wrought 6063-T5 included for comparison purposes.

Temperature	c_p (J·g^{-1}K^{-1})				
Range	PM System				Wrought
(°C)	0.0Sn	0.25Sn	0.5Sn	1.0Sn	6063-T5
100	0.922	0.908	0.940	0.880	0.923
150	0.950	0.950	0.987	0.913	0.973
200	0.970	0.969	1.006	0.927	0.995

Figure 33 presents the average thermal diffusivity of each chemistry as well as that of wrought 6063-T5, across temperatures ranging from ambient to 250°C. Here, obvious differences in diffusivity between the materials were noted. One observation was that data from the Sn-bearing PM alloys were similar and rather tightly clustered. Comparatively, the results for 0.0Sn were significantly lower. This was ascribed to the heightened level of residual porosity in this particular alloy (Figure 30, Figure 32) as pores provide significant impedance to the diffusion of thermal energy. For the tin-containing PM chemistries porosity is likely also the primary culprit for the reduced diffusivity compared to wrought, as any impedance to the diffusion of thermal energy will have an impact. The chemical change in these three chemistries may have also been a contributing factor as elemental tin has a thermal diffusivity nearly half that of 6063.

Figure 33: Thermal diffusivities of PM specimen in the T2 state. Data acquired from wrought 6063-T5 included for comparison purposes.

The points at which thermal conductivity could be calculated for any chemistry in this analysis were limited by the nature of the data collection methods employed for each factor. In this sense, the discrete temperatures at which thermal diffusivity was determined defines the temperatures at which thermal conductivity can be confidently calculated, and the lack of accurate c_p measurements bellow 100°C limited the range even further. However, for the temperatures at which all applicable data were available, values for thermal conductivity were determined as shown in Figure 34. The 0.0Sn chemistry had a thermal conductivity only ~20% less than that of wrought 6063 at the same temperature, despite it's significant level of porosity and thus far lower thermal diffusivity than the tin-bearing chemistries. Overall the 0.5Sn system maintained the highest thermal conductivity with measured values only ~6% lower than that of wrought. Unlike the 0.0Sn system however, this superiority is based primarily on superior specific heat capacity compared to the other

chemistries, as all tin-bearing chemistries shared very similar thermal diffusivity values across all temperatures. With similar reasoning, the 1.0Sn system presented the lowest thermal conductivity due to it possessing the lowest specific heat capacity values across all tested temperatures.
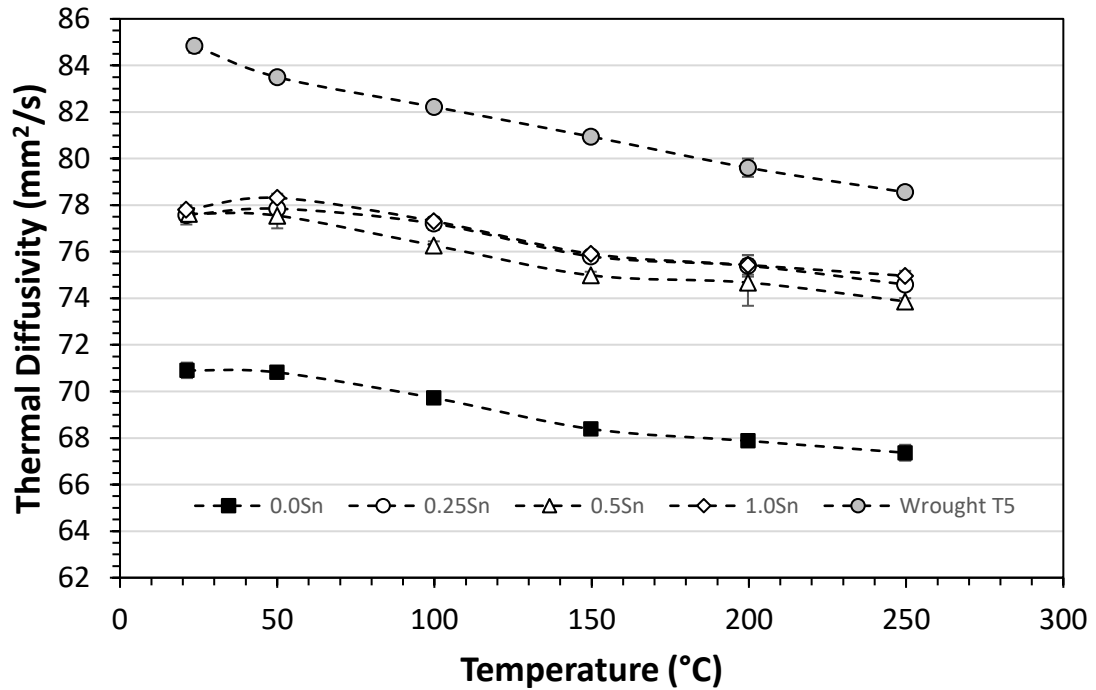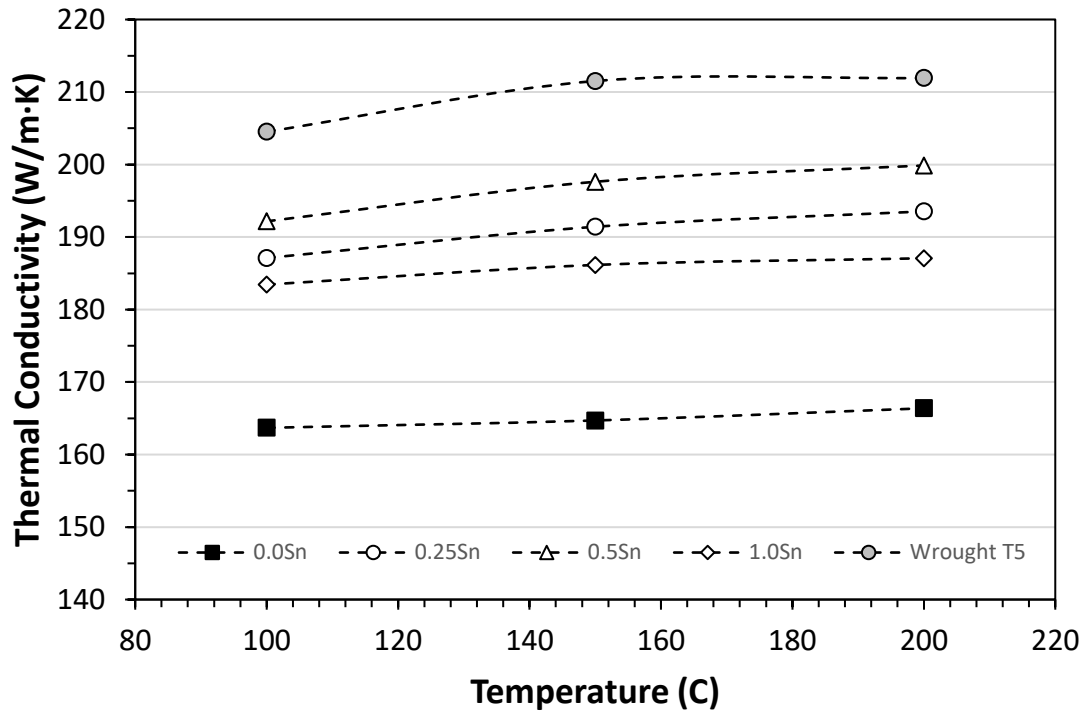

Figure 34: Thermal conductivities of PM specimen in the T2 state. Data acquired from wrought 6063-T5 included for comparison purposes.

3.5 Conclusions

The over-arching objective of this study was to develop an Al-Si-Mg-(Sn) PM that exhibited an acceptable response to PM processing and final properties that were aligned with those of wrought 6063. Through this work the following conclusions were reached:

- Tin additions were imperative for good overall sintering response of this alloy, and manifested heightened levels of densification in sintering.

- Effective processing parameters for the PM systems included a compaction pressure ≥250 MPa, a sintering temperature of ~635°C, and a sintering time of 20 minutes.

- PM systems were receptive to post-sinter sizing coupled with natural aging to the T2 state as manifested by improvements in density and hardness.

- All PM chemistries containing tin exhibited a balanced combination of yield strength (~100MPa), UTS (~130MPa), and ductility (~14%).

- Each of the PM alloy systems containing tin also exhibited thermal conductivities that were >180 $Wm^{-1}K^{-1}$ and as such, were similar to those measured for wrought 6063-T5.

3.6 Acknowledgements

CHPATER 4 – FURTHER ANALYSIS OF HEAT TREATMENT PROCESSING

The mechanical and thermal analysis of the four potential PM counterpart chemistries for Al6063 provided significant confidence that PM processing of such alloys could be prove to be viable as an alternative to wrought Al6063 in some scenarios. Potential for further improvement of a PM counterpart was then explored, with the goal of improving the viability of such a system even further through more controlled thermal and mechanical post-processing. Based on the results of the initial analysis, the 0.5Sn chemistry was selected as the optimal formulation for continued work. This selection was based on 0.5Sn providing the best thermal conductivity across all tested temperatures, from among the four PM chemistries as well as the best tensile properties both in terms of strength and ductility.

4.1 Experimental Procedures

The manufacturing of samples for this continued stage of analysis followed the same parameters outlined in Chapter 3, through to the conclusion of sintering. After which, each sample was processed to the T8 state. Here, samples were first solutionized in a Thermo Scientific Lindberg/Blue M 5.3L C2 Moldatherm Box Furnace at 520°C for two hours, after which they were immediately water quenched. Following this quench samples were then sized to a target reduction of 3.5%, and then artificially aged in a Thermo Scientific Heratherm General Lab Oven at 175°C for 20 hours. The initial T8 parameters were identified through the development of an artificial aging curve with the above parameters across a long range of artificial aging times. The tensile response and thermal properties of the samples produced to T8 specifications were then analyzed as per the procedures outlined in Chapter 3.

4.2 Results and Discussion

4.2.1 Artificial Aging Response

The final stage of the T8 temper process is an artificial aging. An artificial aging curve was developed for the 0.5Sn chemistry over the period of 28 days to identify peak aging state as well as the bounds within which this peak could be achieved. Figure 35 illustrates the results of this analysis, and from it two significant observations can be made. The first is that peak hardness was achieved by the 10 hour mark and was maintained through to the 24 hour mark. Between the 24 and 48 hour mark the hardness began to decrease, indicating the onset of overaging at some point in this range. The second interesting observation is that at every stage in the aging process the hardness of the 0.5Sn chemistry is significantly higher than that achieved through the initial analysis in the T2 state. 0.5Sn in the T2 state for saw a peak hardness of merely 36±6 on the HRE scale, while even just one hour of aging after solutionization and cold working (the first two stages of the T8 treatment process) resulted in a measured hardness of 64±3. This significant difference is primarily a result of the annealed state each sample is initially in upon the conclusion of sintering, due to the non-quenched cooling imparted before removal from the furnace.
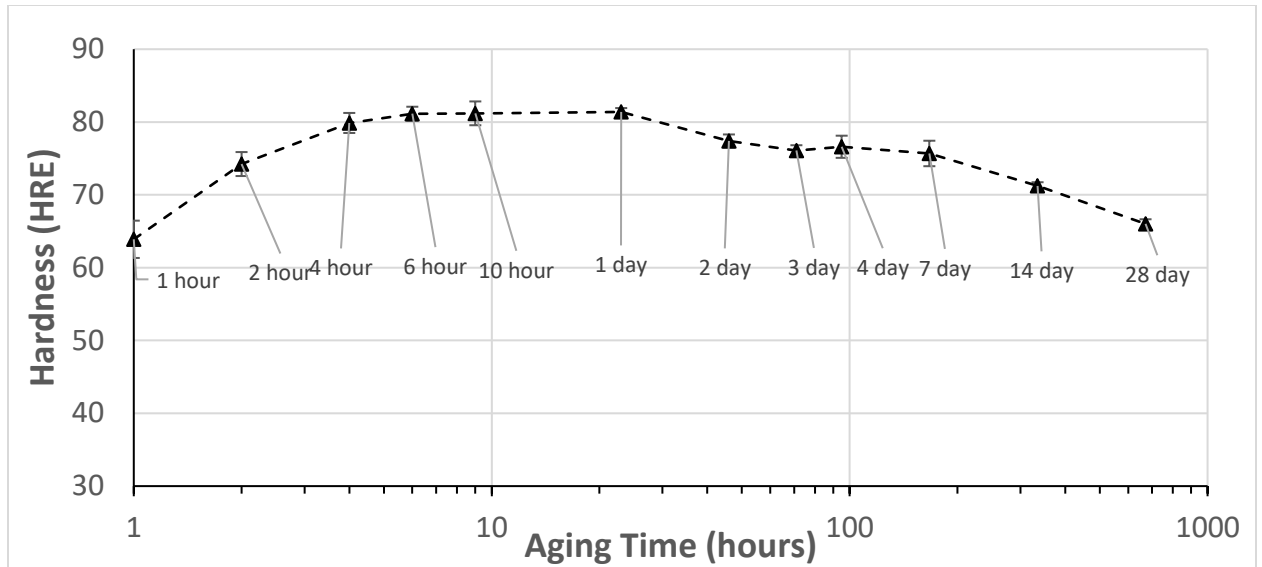
Figure 35: T8 treatment response via hardness testing for the 0.5Sn chemistry, ageing temperature of 175°C

4.2.2 T8 Tensile Response

Analysis of the tensile properties further illustrated the significant change in mechanical properties between the T2 and T8 states. Table 8 lists the tensile properties of the 0.5Sn system in the T8 state, alongside the same chemistry in T2 and wrought Al6063 in T8 for comparison. These results further demonstrate the significant increase in mechanical properties between the two tempers analyzed for the PM systems, with the 0.5Sn chemistry even outperforming the wrought system in terms of yield and tensile strength in this analysis. This significant increase in strength did also coincide with a reduction in ductility of over 50% however.

Table 8: Tensile properties for 0.5Sn chemistry in the T8 state with comparitors

Alloy	E (GPa)	Yield Strength (MPa)	UTS (MPa)	Elongation (%)	Hardness (HRE)
0.5Sn T2	75±6	99±1	134±2	15%±3%	36±6
0.5Sn T8	83±4	208±2	241±1	6%±1%	81±2
Wrought T8	67±3	149±5	233±2	15%±1%	86±3

4.2.3 Thermal Analysis

Further thermal analysis was also conducted on 0.5Sn and wrought samples manufactured to the T8 temper state. With the high value placed on thermal characteristics for this alloy system, each stage in this analysis was conducted in triplicate for the 0.5Sn chemistry, with three distinct samples produced for each stage to the exact same specifications. Table 9 presents the apparent specific heat capacity of each individual 0.5Sn sample tested, along with the wrought T8 sample. The most significant difference of note in the case of c_p is that unlike the samples tested in the T2 state, the general stability of each curve allows for confidence over a much more significant range of temperatures. The lower limit around 90°C is still apparent, however the c_p determination from the curves is not impeded by dips due to thermal events until well above the target temperature range of 100-250°C. This suggests that the calculated thermal conductivity at the highest temperature of 250°C for this chemistry can be considered a viable result, unlike the T2 state in the initial analysis.

Table 9: Measured heat capacities at the target temperatures for 0.5Sn PM specimens in the T8 state.Data acquired for wrought 6063-T8 included for comparison purposes.

Temperature Range (°C)	c_p (J·g^{-1}K^{-1})			
	PM System			*Wrought*
	0.5Sn T8_1	0.5Sn T8_2	0.5Sn T8_3	*6063-T8*
100	0.916	0.916	0.833	0.942
150	0.965	0.969	0.892	1.004
200	0.979	0.995	0.920	1.039
250	1.009	1.037	0.949	1.090

As with the determination of c_p, the thermal diffusivity was quantified three separate times with three discrete samples of 0.5Sn T8, however in Figure 36 the three distinct runs have already been combined for ease of visualization. The T8 temper does result in a consistent increase in thermal diffusivity across the entire temperature range, likely due to the greater overall homogeneity of the alloy system resultant from the solutionization phase in the T8 temper process.

Figure 36: Thermal Diffusivities of 0.5Sn and Wrought Al6063, comparison of T8 state with As-sintered/As-received state

Figure 37 presents the thermal conductivity of the 0.5Sn T8 chemistry alongside the original T2 data and wrought T8 for comparison. Unlike the previous analysis of the T2 state, higher confidence in the determined heat capacity of the PM system in the T8 state allowed for the confident determination of thermal conductivity at the 250°C mark in addition to the lower temperatures explored previously. The 0.5Sn T2 values are truncated in Figure 37 as to only include confident values from the prior analysis.

The consistency in trend for the T8 values versus the T2 values at the 250°C mark is a product of the consistency in c_p through and beyond this temperature for the samples in the T8 state, where thermal events were distorting the c_p evaluation for the T2 analysis. This lends further support to the assertion in the earlier analysis that the values presented at 250°C for the T2 analysis were not truly indicative of the thermal conductivity at that temperature.
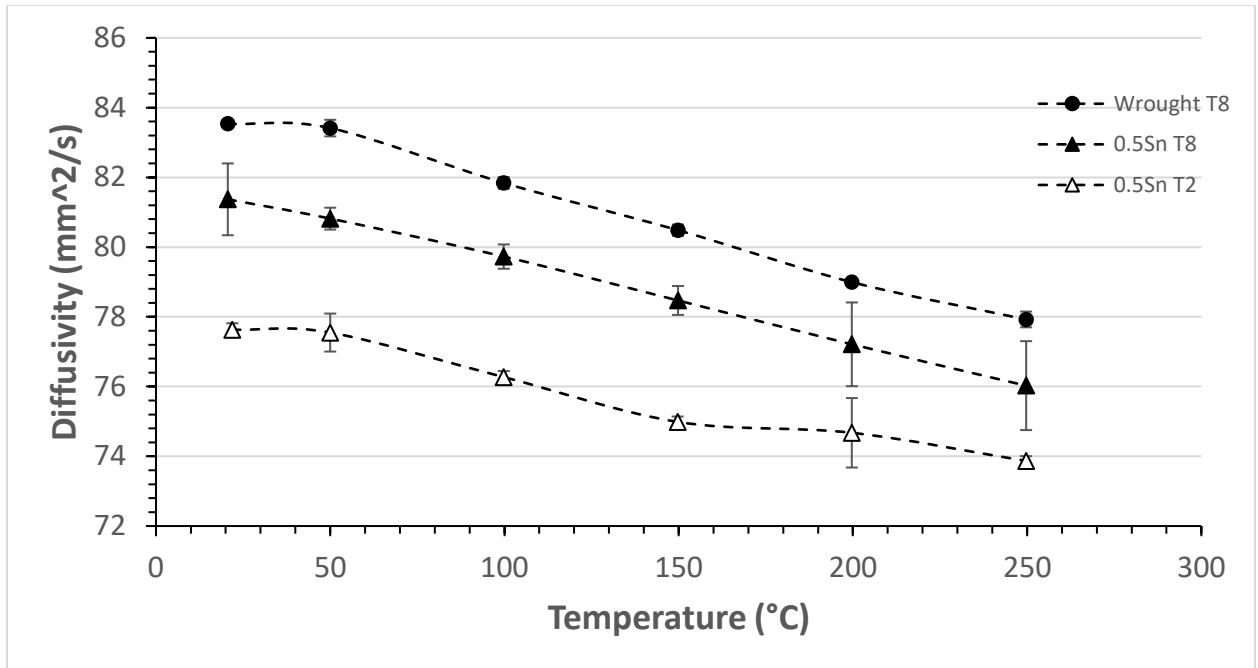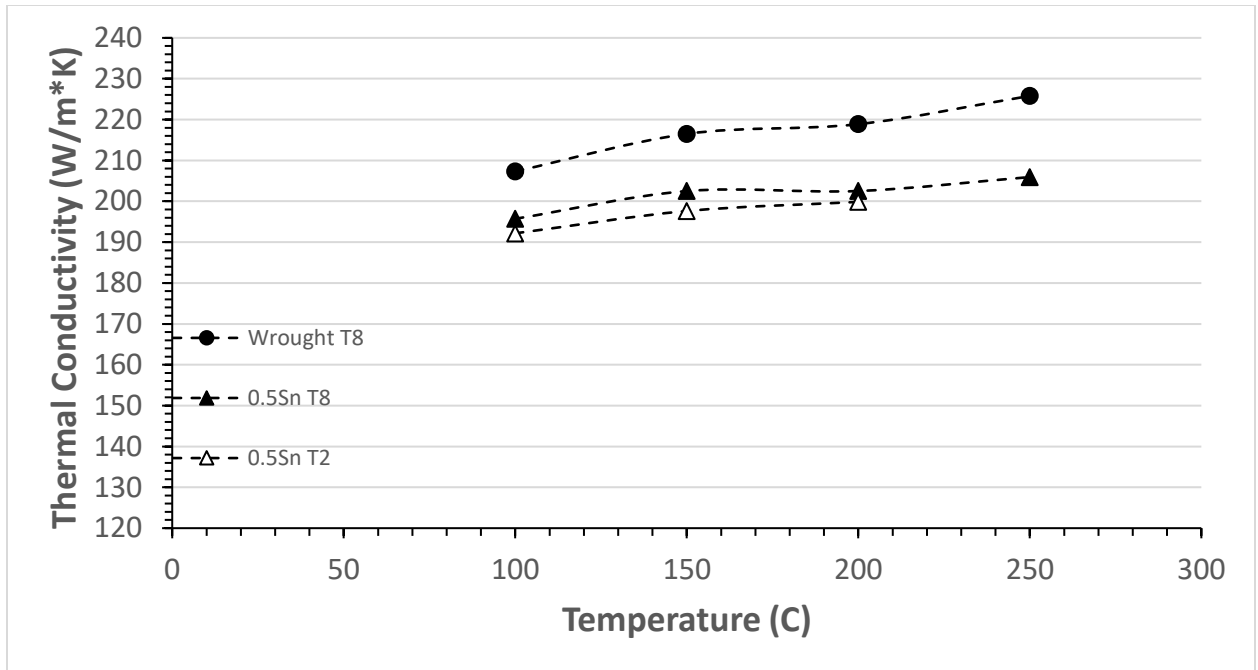
Figure 37: Thermal Conductivities of 0.5Sn and Wrought Al6063, comparison of T8 state with As-sintered/As-received state

When all above confidently determined values were considered, it was found that there was not a significant improvement in thermal conductivity between the two temper states. This does not take away from the extremely strong response for the 0.5Sn chemistry in both tempers; 94% of wrought in the T8 state and 92% of wrought in the T2 state at 100°C. Furthermore, while the T8 temper does not provide significant improvement to thermal conductivity, it does provide significant improvement to material strength. The 0.5Sn chemistry PM counterpart to Al6063 in a T8 temper provides improvements to both thermal and mechanical properties without the need to compromise either area (with the exception of reducing ductility), making it a very promising material for potential utilization in place of wrought Al6063 for some applications.

CHAPTER 5 – SUMMARY AND CONCLUSIONS

To summarize, this research has provided a thorough evaluation of the viability of a PM analogue to wrought aluminum alloy 6063 (Al-0.7Mg-0.5Si). The analysis of this lean 6xxx series alloy was conducted with the intention of expanding the range of available aluminum alloys for PM manufacturing. Through the development of new formulations, gaps in applicability for PM aluminum can be filled with new alternatives with high viability in terms of both mechanical and thermal characteristics. This specific body of work focused on thorough analysis and comparison of four PM chemistries all based on the 6063 system. Each system was based on the same original chemistry (Al-0.7Mg-0.5Si), achieved through the blending of elemental aluminum powder, prealloyed Al-12Si powder, and elemental magnesium powder. Furthermore, three of the four chemistries additionally contained varied quantities of tin to the ratios of 0.25wt%, 0.5wt%, or 1.0wt%, all achieved through addition of elemental tin powder. The four chemistries for analysis were thus referred to by their tin content throughout the analysis; 0.0Sn, 0.25Sn, 0.5Sn, and 1.0Sn.

Initial stages of analysis focused on tracking the sintering response of each of the four chemistries across significantly varied sintering conditions, with the goal of identifying optimal sintering parameters for this system. The impacts of sintering temperature, compaction pressure, and sintering time, were each independently ganalyzed, with respective values from low to high extremes in each case (610-640°C, 150-550 MPa, 5-30 minutes, respectively). Across the three parameters, alongside the identification of optimal values a number of patterns were identified between the four chemistries. The most striking overall observation is consistent confirmation that the presence of tin as a sintering aid in these alloy systems was imperative to achieve good sintering response, regardless of specific parameters. Across all three stages of analysis, the 0.0Sn chemistry performed well below the tin-containing chemistries achieving significantly lower densification and hardness. Across the tin bearing chemistries, sintering temperature produced the widest range of results within the tin-bearing chemistries. Parameters for which peak properties are achieved are consistent across all three tin-bearing chemistries, with 0.25Sn and 0.5Sn

consistently performing very slightly better than the 1.0Sn chemistry. For all three chemistries peak properties can be achieved with the same range of parameters, 630-640°C sintering temperature, a compaction pressure of 350MPa or greater, and a sintering time between 10 and 30 minutes. Optimal Sintering temperature and time values were selected from within these ranges to ensure that any minor fluctuation during processing would not have any impact. Thus, selected parameters for these 6063 analogues were a compaction pressure of 350 MPa, followed by sintering at 635°C for 20 minutes.

With confirmation that appreciable densification can be achieved via conventional sintering processes, examination of sizing response and further analysis of microstructure followed. An extended natural aging analysis was conducted to track natural aging characteristics of the alloy systems, indicating that significant natural hardening did not initiate until after 24 hours post-sinter. Therefore optimal sizing response can be achieved with sizing within the 24 hour period after sintering, and all future analysis saw sizing completed in this time frame. In this state, sizing results in the equivalent of a T2 temper for the PM systems. Sizing in this state is valuable for achieving exact dimensional tolerances, but it was found that it provided very minimal further densification overall, and relatively small improvement in hardness.

Further analysis of the PM alloy systems were carried out on in two distinct sections. The first saw analysis of samples produced in the T2 state as described above, and the later saw analysis of 0.5Sn samples produced in the T8 state. To achieve a T8 temper samples prepared using the above parameters were then solutionized, water quenched, sized, and then artificially aged at 175°C for 20 hours.

The tensile response of the PM systems was examined for all chemistries in the T2 state, as well as the 0.5Sn chemistry in the T8 state. The high level of porosity in 0.0Sn lead to significantly weaker tensile properties than the three tin-bearing chemistries, particularly in terms of maximum elongation. All PM systems in the T2 state performed worse than wrought in terms of yield and ultimate tensile strength, 0.5Sn achieving 68% and 72% of

wrought respectively. However, in terms of elongation the tin-containing PM systems performed exactly in line with wrought. The T8 temper resulted in significant change in all tensile and hardness properties for the 0.5Sn system. The 0.5Sn T8 system achieved similar ultimate tensile strength to wrought in the same T8 state, and exceeded wrought T8 in yield strength in this analysis. A reduction in maximum elongation of over 50% was also observed.

The thermal properties of these PM systems were of great importance for this analysis, good thermal conductivity was a highly important requirement for determining the viability of this PM system. Thermal property analysis carried out on the four chemistries in the T2 state, as well as the 0.5Sn chemistry in the T8 state. The determination of thermal conductivity required the determination of coefficient of thermal expansion via thermal dilatometry, determination of specific heat capacity via differential scanning calorimetry, and the determination of thermal diffusivity via laser flash analysis. Differences in the operation and data collection methods for each system, coupled with limitations in how each system operates, constrained the temperature range in which thermal conductivity could be confidently calculated. While limited to select discrete temperatures above 100°C, the final thermal conductivity values indicated very promising results. The 0.0Sn chemistry performed worst due to it's high level of porosity and thus far lower thermal diffusivity compared to the tin-bearing systems or wrought. None the less, 0.0Sn T2 still achieved thermal conductivity only 20% lower than that of wrought 6063 at 100°C. All three of the tin-bearing chemistries saw better performance, with 0.5Sn T2 performing best with a thermal conductivity of 192 W/m·K at 100°C, just 6% lower than wrought at the same temperature. 0.5Sn in the T8 state did not see any significant change in thermal conductivity compared to T2, however.

Overall it has been determined that with a small fractional addition of tin, a PM system with a bulk chemistry matching that of aluminum alloy 6063 has shown great promise as a viable PM analogue. An alloy system containing an addition of 0.5wt% tin and treated in

the T8 state offers excellent thermal properties compared to wrought alongside similarly promising mechanical properties.

5.1 Future Work

Potential future research recommendations include:

1. Analysis of thermal properties at room temperature, requiring capability for c_p determination at lower temperatures.
2. Chemistry modifications; exploration of impact tin has on available magnesium content for magnesium silicide precipitate formation, and potential benefit of increasing magnesium content in alloy system.
3. Further analysis into required quantity of tin addition for systems manufactured under these peak conditions, to identify a more refined target for tin quantity.
4. More specifically identify the impact of tin presence on the thermal properties of the alloy systems, beyond it's densification benefits.
5. Expansion of thermal analysis across wider range of processing parameters and chemical compositions to expand range of viable production.

References

[1]   R. M. German, *Powder Metallurgy Science*, 2nd ed. Princeton, New Jersey: Metal Powder Industries Federation, 1984.

[2]   ASM International, *ASM Handbook Volume 7 - Powder Metal Technologies and Applications*. Materials Park, Ohio: ASM International, 1998.

[3]   Y. W. Kim, W. M. Griffith, and F. H. Froes, "Surface Oxides in P/M Aluminum Alloys," *JOM*, vol. 37, no. 8, pp. 27–33, Aug. 1985.

[4]   R. N. Lumley, *Fundamentals of aluminium metallurgy: Production, processing and applications*. Cambridge, UK: Woodhead Publishing Limited, 2010.

[5]   T. B. Sercombe and G. B. Schaffer, "On the use of trace additions of Sn to enhance sintered 2xxx series Al powder alloys," *Mater. Sci. Eng. A*, vol. 268, no. 1–2, pp. 32–39, 1999.

[6]   B. J. Hall and G. B. Schaffer, "Statistical experimental design of Al-Cu-Mg-Si P/M alloys," *J. Light Met.*, vol. 2, no. 4, pp. 229–238, Nov. 2002.

[7]   A. D. P. LaDelpha, M. P. Mosher, W. F. Caley, G. J. Kipouros, and D. P. Bishop, "On the simulation of wrought AA4032 via P/M processing," *Mater. Sci. Eng. A*, vol. 479, no. 1–2, pp. 1–9, Apr. 2008.

[8]   D. P. Bishop, W. F. Caley, G. J. Kipouros, R. L. Hexemer, and I. W. Donaldson, "Powder metallurgy processing of 2xxx and 7xxx series Aluminium alloys," in *Canadian Metallurgical Quarterly*, 2011, vol. 50, no. 3, pp. 246–252.

[9]   C. D. Boland, D. P. Bishop, R. L. Hexemer, and I. W. Donaldson, "On the development of an aluminum PM alloy for 'press-sinter- size' technology," *Adv. Powder Metall. Part. Mater. - 2010, Proc. 2010 Int. Conf. Powder Metall. Part. Mater. PowderMet 2010*, no. June 2010, pp. 764–777, 2010.

[10] L. J. B. Smith, S. F. Corbin, R. L. Hexemer, I. W. Donaldson, and D. P. Bishop, "Development and processing of novel aluminum powder metallurgy materials for heat sink applications," *Metall. Mater. Trans. A Phys. Metall. Mater. Sci.*, vol. 45, no. 2, pp. 980–989, 2014.

[11] R. N. Lumley, T. B. Sercombe, and G. B. Schaffer, "Surface oxide and the role of magnesium during the sintering of aluminum," *Metall. Mater. Trans. A Phys. Metall. Mater. Sci.*, vol. 30, no. 2, pp. 457–463, 1999.

[12] T. B. Sercombe, "On the sintering of uncompacted, pre-alloyed Al powder alloys," *Mater. Sci. Eng. A*, vol. 341, no. 1–2, pp. 163–168, Jan. 2003.

[13] G. B. Schaffer, J. Y. Yao, S. J. Bonner, E. Crossin, S. J. Pas, and A. J. Hill, "The effect of tin and nitrogen on liquid phase sintering of Al-Cu-Mg-Si alloys," *Acta Mater.*, vol. 56, no. 11, pp. 2615–2624, 2008.

[14] M. Youseffi and N. Showaiter, "PM processing of elemental and prealloyed 6061 aluminium alloy with and without common lubricants and sintering aids," *Powder Metall.*, vol. 49, no. 3, pp. 240–252, Sep. 2006.

[15] N. Showaiter and M. Youseffi, "Compaction, sintering and mechanical properties of elemental 6061 Al powder with and without sintering aids," *Mater. Des.*, vol. 29, no. 4, pp. 752–762, 2008.

[16] L. P. Lefebvre, Y. Thomas, and B. White, "Effects of lubricants and compacting pressure on the processability and properties of aluminum P/M parts," *J. Light Met.*, vol. 2, no. 4, pp. 239–246, Nov. 2002.

[17] R. M. German, P. Suri, and S. J. Park, "Review: Liquid phase sintering," *J. Mater. Sci.*, vol. 44, no. 1, pp. 1–39, 2009.

[18] H. Momeni, H. Razavi, and S. G. Shabestari, "Effect of supersolidus liquid phase sintering on the microstructure and densification of the Al-Cu-Mg pre-alloyed powder," *Iran. J. Mater. Sci. Eng.*, vol. 8, no. 2, pp. 10–17, 2011.

[19] M. Youseffi, N. Showaiter, and M. T. Martyn, "Sintering and mechanical properties of prealloyed 6061 Al powder with and without common lubricants and sintering aids," *Powder Metall.*, vol. 49, no. 1, pp. 86–95, Mar. 2013.

[20] ASM International, *ASM Handbook Volume 3 - Alloy Phase Diagrams*. Materials Park, Ohio, 1998.

[21] T. Pieczonka, T. Schubert, S. Baunack, and B. Kieback, "Sintering Behaviour of Aluminium in Different Atmospheres," no. August 2016, pp. 5–8, 2005.

[22] T. Schubert, T. Pieczonka, S. Baunack, and B. Kieback, "The Influence of the Atmosphere and Impurities on the Sintering Behaviour of Aluminium," 2005.

[23] G. B. Schaffer and B. J. Hall, "The influence of the atmosphere on the sintering of aluminum," *Metall. Mater. Trans. A Phys. Metall. Mater. Sci.*, vol. 33, no. 10, pp. 3279–3284, 2002.

[24] I. A. MacAskill, R. L. Hexemer, I. W. Donaldson, and D. P. Bishop, "Effects of magnesium, tin and nitrogen on the sintering response of aluminum powder," *J. Mater. Process. Technol.*, vol. 210, no. 15, pp. 2252–2260, Nov. 2010.

[25] Z. Z. Fang, *Sintering of Advanced Materials*. Cambridge, UK: Woodhead Publishing Limited, 2010.

[26] A. Ibrahim, D. P. Bishop, and G. J. Kipouros, "Sinterability and characterization of commercial aluminum powder metallurgy alloy Alumix 321," *Powder Technol.*, vol. 279, pp. 106–112, Jul. 2015.

[27] G. B. Schaffer, T. B. Sercombe, and R. N. Lumley, "Liquid phase sintering of aluminium alloys," vol. 67, pp. 85–91, 2001.

[28] D. P. Bishop, R. L. McNalley Jr., and T. E. Geiman, "METALLURGICAL CONSIDERATIONS IN THE MANUFACTURE AND DEVELOPMENT OF ALUMINUM P/M CAMSHAFT BEARING CAPS D.P.," pp. 1535–1540, 2005.

[29] M. Harding, I. Donaldson, R. Hexemer Junior, and D. Bishop, "Effects of Post-Sinter Processing on an Al–Zn–Mg–Cu Powder Metallurgy Alloy," *Metals (Basel).*, vol. 7, no. 9, p. 370, Sep. 2017.

[30] W. F. Smith, *Structure and Properties of Engineering Alloys.pdf*, 2nd Ed. McGraw-Hill Inc., 1993.

[31] University of Cambridge, "DoITPoMS - TLP Library Solid Solutions - Precipitates," *Dissemination of IT for the Promotion of Materials Science*, 2020. [Online]. Available: https://www.doitpoms.ac.uk/tlplib/solid-solutions/precipitates.php. [Accessed: 28-Oct-2020].

[32] H. K. Khaira, "Precipitation Hardening," Bhopal, 2013.

[33] A. P. Mouritz, Ed., *Introduction to Aerospace Materials*. Woodhead Publishing, 2012.

[34] H. K. D. . Bhadeshia, "Precipitate free zones," *Phase Transformations & Complex Properties Research Group*. University of Cambridge.

[35] L. Zhen, W. D. Fei, S. B. Kang, and H. W. Kim, "Precipitation behaviour of Al-Mg-Si alloys with high silicon content," *J. Mater. Sci.*, vol. 32, no. 7, pp. 1895–1902, 1997.

[36]   J. P. Lynch, L. M. Brown, and M. H. Jacobs, "Microanalysis of age-hardening precipitates in aluminium alloys," *Acta Metall.*, vol. 30, no. 7, pp. 1389–1395, Jul. 1982.

[37]   S. J. Andersen, C. D. Marioara, J. Friis, S. Wenner, and R. Holmestad, "Precipitates in aluminium alloys," 2018.

[38]   H. Zhu, M. J. Couper, and A. K. Dahle, "Effect of process variables on Mg-Si particles and extrudability of 6xxx series aluminum extrusions," *JOM*, vol. 63, no. 11, pp. 66–71, Nov. 2011.

[39]   H. Zhong, P. A. Rometsch, and Y. Estrin, "The influence of Si and Mg content on the microstructure, tensile ductility, and stretch formability of 6xxx alloys," *Metall. Mater. Trans. A Phys. Metall. Mater. Sci.*, vol. 44, no. 8, pp. 3970–3983, Aug. 2013.

[40]   A. K. Gupta, D. J. Lloyd, and S. A. Court, "Precipitation hardening in Al-Mg-Si alloys with and without excess Si," *Mater. Sci. Eng. A*, vol. 316, no. 1–2, pp. 11–17, Oct. 2001.

[41]   M. Murayama, K. Hono, W. Miao, and D. E. Laughlin, "The effect of Cu additions on the precipitation kinetics in an Al-Mg-Si alloy with excess Si," *Metall. Mater. Trans. A Phys. Metall. Mater. Sci.*, vol. 32, no. 2, pp. 239–246, 2001.

[42]   K. M. C. Wong, A. R. Daud, and A. Jalar, "Microhardness and tensile properties of a 6XXX alloy through minor additions of Zr," *J. Mater. Eng. Perform.*, vol. 18, no. 1, pp. 62–65, Feb. 2009.

[43]   G. Mrówka-Nowotnik, "Influence of chemical composition variation and heat treatment on microstructure and mechanical properties of 6xxx alloys," 2010.

[44] W. F. Miao and D. E. Laughlin, "Effects of Cu content and preaging on precipitation characteristics in aluminum alloy 6022," *Metall. Mater. Trans. A Phys. Metall. Mater. Sci.*, vol. 31, no. 2, pp. 361–371, 2000.

[45] H. Zhong, P. Rometsch, and Y. Estrin, "Effect of alloy composition and heat treatment on mechanical performance of 6xxx aluminum alloys," *Trans. Nonferrous Met. Soc. China (English Ed.*, vol. 24, no. 7, pp. 2174–2178, Jul. 2014.

[46] P. E. Fortin, "A precipitation hardening phenomenon in aluminum-magnesium-silicon alloys," *Can. Metall. Q.*, vol. 2, no. 2, pp. 143–155, Apr. 1963.

[47] ASM International, *ASM Handbook Volume 2 - Properties and Selection: Nonferrous Alloys and Special-Purpose Materials*. Materials Park, Ohio: ASM International, 1990.

[48] D. Halliday, R. Resnick, and J. Walker, *Fundamentals of Physics: Extended*, 11th Editi. Wiley & Sons, Inc., 2018.

[49] R. B. Cassel, "How Tzero^{TM} Technology Improves DSC Performance Part III: The Measurement of Specific Heat Capacity."

[50] P. Šimon and Z. Cibulková, "MEASUREMENT OF HEAT CAPACITY BY DIFFERENTIAL SCANNING CALORIMETRY."

[51] K. L. Ramakumar, M. K. Saxena, and S. B. Deb, "Experimental evaluation of procedures for heat capacity measurement by differential scanning calorimetry," *J. Therm. Anal. Calorim.*, vol. 66, no. 2, pp. 387–397, 2001.

[52] ASTM International, *E1269-11(2018) Standard Test Method for Determining Specific Heat Capacity by Differential Scanning Calorimetry*. West Conshohocken, PA: ASTM International, 2018.

[53] D. W. Hahn and M. N. Özisik, *Heat Conduction, 3rd Edition*. Wiley & Sons, Inc., 2012.

[54] MaxwellMolecule, "Simple definition of thermal conductivity (Diagram)." 2019.

[55] R. B. Bird, W. E. Stewart, and E. N. Lightfoot, *Transport Phenomena, Revised 2nd Edition*. Wiley & Sons, Inc., 2006.

[56] The McGraw-Hill Companies, *McGraw-Hill Dictionary of Scientific & Technical Terms, 6E*. The McGraw-Hill Companies, 2003.

[57] M. Worgull, "Molding Materials for Hot Embossing," in *Hot Embossing*, Elsevier, 2009, pp. 57–112.

[58] N. Yüksel, "The Review of Some Commonly Used Methods and Techniques to Measure the Thermal Conductivity of Insulation Materials," in *Insulation Materials in Context of Sustainability*, InTech, 2016.

[59] W. J. Parker, R. J. Jenkins, C. P. Butler, and G. L. Abbott, "Flash method of determining thermal diffusivity, heat capacity, and thermal conductivity," *J. Appl. Phys.*, vol. 32, no. 9, pp. 1679–1684, Sep. 1961.

[60] B. Lin, C. Li, C. Su, H. Ban, R. N. Scripa, and S. L. Lehoczky, "Method for obtaining thermal conductivity from modified laser flash measurement," in *American Society of Mechanical Engineers, Heat Transfer Division, (Publication) HTD*, 2005, vol. 376 HTD, no. 2, pp. 725–730.

[61] J. D. James, J. A. Spittle, S. G. R. Brown, and R. W. Evans, "A review of measurement techniques for the thermal expansion coefficient of metals and alloys at elevated temperatures," *Measurement Science and Technology*, vol. 12, no. 3. IOP Publishing Ltd, pp. 1–15, 01-Mar-2001.

[62] C. P. Romao, K. J. Miller, C. A. Whitman, M. A. White, and B. A. Marinkovic, "Negative Thermal Expansion (Thermomiotic) Materials," in *Comprehensive Inorganic Chemistry II (Second Edition): From Elements to Applications*, vol. 4, Elsevier Ltd, 2013, pp. 127–151.

[63] R. Nave, "Thermal Expansion," *HyperPhysics, University of Georgia*, 2017. [Online]. Available: http://hyperphysics.phy-astr.gsu.edu/hbase/thermo/thexp.html#c1. [Accessed: 25-Nov-2020].

[64] R. E. Wetton, "Chapter 6 Thermomechanical Methods," in *Handbook of Thermal Analysis and Calorimetry*, vol. 1, Elsevier, 1998, pp. 363–399.

[65] P. Zhang, "Transducers and valves," in *Advanced Industrial Control Technology*, Elsevier, 2010, pp. 117–152.

[66] NETZSCH, "Dilatometry - NETZSCH Thermal Academy." [Online]. Available: https://www.netzsch-thermal-academy.com/en/advanced-materials-testing/methods/dilatometry/. [Accessed: 30-Nov-2020].

[67] W. D. Judge, D. P. Bishop, and G. J. Kipouros, "Industrial Sintering Response and Microstructural Characterization of Aluminum Powder Metallurgy Alloy Alumix 123," *Metallogr. Microstruct. Anal.*, vol. 6, no. 5, pp. 375–382, Oct. 2017.

[68] R. E. D. Mann, R. L. Hexemer, I. W. Donaldson, and D. P. Bishop, "Hot deformation of an Al-Cu-Mg powder metallurgy alloy," *Mater. Sci. Eng. A*, vol. 528, no. 16–17, pp. 5476–5483, Jun. 2011.

[69] R. W. Cooke, R. L. Hexemer, I. W. Donaldson, and D. P. Bishop, "Dispersoid strengthening of Al–Cu–Mg P/M alloy utilising transition metal additions," *http://dx.doi.org/10.1179/1743290111Y.0000000012*, vol. 55, no. 3, pp. 191–199, Jul. 2013.

[70] I. A. MacAskill, A. D. P. Ladepha, J. H. Milligan, J. J. Fulton, and D. P. Bishop, "Effects of cold and hot densification on the mechanical properties of a 7XXX series powder metallurgy alloy," *Powder Metall.*, vol. 52, no. 4, pp. 304–310, Dec. 2009.

[71] A. Arockiasamy *et al.*, "Sintering behaviour of Al-6061 powder produced by rapid solidification process," *Powder Metall.*, vol. 54, no. 3, pp. 354–359, Jul. 2011.

[72] P. R. S. Kumar, S. Kumaran, and T. S. Rao, "Comparison study of fly ash reinforced AA6061 composites using press sinter extrusion and press extrusion approaches," *Powder Metall.*, vol. 53, no. 2, pp. 163–168, Jun. 2010.

[73] J. Zhang and A. Gao, "Effect of heat treatment on thermal conductivity of 6063 aluminum alloy," in *2011 2nd International Conference on Mechanic Automation and Control Engineering, MACE 2011 - Proceedings*, 2011, pp. 6449–6451.

[74] Metal Powder Industries Federation, "STANDARD TEST METHOD 42: METHOD FOR DETERMINATION OF DENSITY OF COMPACTED OR SINTERED POWDER METALLURGY (PM) PRODUCTS MATERIALS," 2022.

[75] ASTM International, "E8/E8M − 16a Standard Test Methods for Tension Testing of Metallic Materials 1," 2016.

[76] G. A. W. Sweet, B. W. Williams, A. Taylor, R. L. Hexemer, I. W. Donaldson, and D. P. Bishop, "A microstructural and mechanical property investigation of a hot upset forged 2xxx series aluminum powder metallurgy alloy reinforced with AlN," *J. Mater. Process. Technol.*, vol. 284, Oct. 2020.